ERDC/CHL TR-12-18

Coastal and Hydraulics Laboratory

US Army Corps
of Engineers®
Engineer Research and
Development Center

# Dredged Material Placement Site Capacity Analysis for Navigation Improvement Project at Grays Harbor, WA

Earl Hayter, Jarrell Smith, David Michalsen, Zeki Demirbilek, and Lihwa Lin

September 2012

ERDC/CHL TR-12-18
September 2012

# Dredged Material Placement Site Capacity Analysis for Navigation Improvement Project at Grays Harbor, WA

Earl Hayter, Jarrell Smith, Zeki Demirbilek, and Lihwa Lin

*Coastal and Hydraulics Laboratory*
*U.S. Army Engineer Research and Development Center*
*3909 Halls Ferry Road*
*Vicksburg, MS 39180-6199*

David R. Michalsen

*U.S. Army Corps of Engineers Seattle District*
*P.O. Box 3755*
*Seattle. WA 98124-3755*

Final report



Prepared for U.S. Army Corps of Engineers, Seattle District
P.O. Box 3755
Seattle. WA 98124-3755

# Abstract

The U.S. Army Engineer District, Seattle requested that the U.S. Army Engineer Research and Development Center, Coastal and Hydraulics Laboratory perform a numerical modeling study for the purpose of performing a dredged material placement (DMP) site capacity analysis for a Navigation Improvement Project for the Federal Navigation Project at Grays Harbor (GH), WA. The project would deepen the inner harbor channel reaches up to two additional feet to reach the authorized project depth of -38 feet. This would require dredging up to an additional 1.7 million cubic yards (MCY) in addition to the 2.8 MCY available for dredging through the Corps O&M program. A project goal is to maximize the dredge volume capacity within existing open water sites while ensuring navigation safety. This study provides estimate of the short-term and long term fate of channel deepening sediments as well as the annual O&M dredge material placed at the DMP sites in the entrance channel to GH. The model simulations indicated a) potential navigation obstruction for the scenario with additional 2.0 MCY; b) potential obstruction for the scenario with additional 1.0 MCY; and c) channel obstructions were significantly reduced at the PCDS for Scenario 3 where the maximum channel obstruction was 170 ft. Two recommendations are made: a) Scenario 3 is preferred as it produces a minimal obstruction to the navigation channel and less channel sedimentation; and b) Modify placement strategy at the SJDS by placing more material in the eastern half than in the western half of the site rather than the uniform placement strategy used at present.

# Contents

# Figures and Tables

## Figures



## Tables

# Preface

The modeling investigation presented in this report was authorized by the U.S. Army Corps of Engineers Seattle District (NWS) to perform dredged material placement site capacity analysis for a Navigation Improvement Project for the Federal Navigation Project at Grays Harbor, WA. David R. Michalsen was the NWS study manager and technical coordinator. The technical work was performed by Earl Hayter, Jarrell Smith, David Michalsen, Zeki Demirbilek and Lihwa Lin. This work was performed at the Coastal and Hydraulics Laboratory (CHL) of the U. S. Army Engineer Research and Development Center (ERDC) during the period of July 2011 to June 2012 under the direction of Ty Wamsley, Chief of Coastal Processes Branch; Pat McKinney, Chief of Field Data Collection and Analysis Branch; Dr. Jackie Pettway, Chief of the Entrances, Harbors and Structures Branch; Bruce Ebersole, Chief of the Flood and Storm Protection Division; Rose Kress, Chief of the Navigation Division, Jose Sanchez; Deputy Director, and William D. Martin, Director of CHL.

COL Kevin J. Wilson was the Commander and Executive Director of ERDC, and Dr. Jeffery P. Holland was the Director.

# Unit Conversion Factors

| Multiply | By | To Obtain |
|---|---|---|
| cubic yards | 0.7645549 | cubic meters |
| feet | 0.3048 | meters |
| miles (U.S. statute) | 1,609.347 | meters |
| yards | 0.9144 | meters |

# Executive Summary

## Background

The U.S. Army Engineer District, Seattle (NWS) requested that the U.S. Army Engineer Research and Development Center (ERDC), Coastal and Hydraulics Laboratory (CHL) perform a numerical modeling study for the purpose of performing a dredged material placement (DMP) site capacity analysis for a Navigation Improvement Project for the Federal Navigation Project at Grays Harbor (GH), Washington. The project would deepen the inner harbor channel reaches (South Reach, Crossover Reach, North Reach, Hoquiam Reach, and Cow Point) up to two additional feet to reach the authorized project depth of -38 feet. This would require dredging up to an additional 1.7 million cubic yards (MCY) in addition to the 2.8 million cubic yards available for dredging through the Corps Operations and Maintenance program. This additional volume of dredged material would need to be placed within the current open water Dredge Material Placement (DMP) sites or one existing offshore placement sites utilized during phase 1 of the deepening which was completed in 1990. The latter would require site redesignation by the resource agencies, have higher transport cost, and result in a net loss of sediment from the system and thus is considered undesirable. Thus a primary project goal is maximizing the dredge volume capacity within the existing open water sites while ensuring navigation safety.

## Purpose of study

This study employs hydrodynamic and sediment transport models to estimate the dynamic capacity of the current open water DMP sites located at the harbor mouth, the South Jetty Disposal Site (SJDS) and the Point Chehalis Disposal Site (PCDS) respectively. The dynamic capacity for three scenarios was determined by including the dispersive nature of dredged material from waves and tidal currents. The first two scenarios included placement of an additional 1) 2.0 MCY, and 2) 1.0 MCY of channel deepening dredged material at the SJDS and PCDS. The third scenario included placement of an additional 2.0 MCY and the PCDS was moved to the north 1000 ft (305 m) and the area designated for dredged material placement was the full site (5000 ft (1524 m) long and 2000 ft (610 m) wide).

This was performed by modeling short and long term fate of dredge material over a projected 10 month project construction window. Previous investigations at GH, including the study reported by Demirbilek et al. (2010), have generated considerable information and predictive capability concerning the behavior of the navigation channel and dredge material fate and transport. The outcomes of previous studies have benefited the present modeling effort. The present study was conducted as a multi-disciplinary approach, making full use of the hydrodynamic, wave, and sediment transport models developed by Demirbilek et al. (2010) in the previous study.

## Wave and hydrodynamic modeling

The height and direction of waves approaching the GH navigation channel change due to wave shoaling, refraction, diffraction, reflection, and breaking. Waves propagating through the entrance interact with the bathymetry, surrounding land features, currents and coastal structures and contribute to bed shear stress and sediment mobility. A spectral wave model was necessary for this project given the large extent of modeling domain over which wave estimates were required. The spectral wave model, CMS-Wave, based on the wave-action balance equation, was used in this study to simulate steady-state spectral transformation of directional random waves in the GH estuary. Details of the wave modeling performed in this study using CMS-Wave for the 10-month dredging window are provided in Chapters 2 and 3 of this report.

The hydrodynamic model used in this study is ADCIRC. It is a finite element model for solving two-dimensional horizontal shallow water equations to calculate the variation in the water surface elevation ($\eta$) and velocities ($u$, $v$). Regional ADCIRC modeling provided regional and local scale water level and velocity fields required for sediment transport modeling in GH. Additional information on features of ADCIRC model, including its governing equations can be found in several references and from the model's home page. Details of the ADCIRC modeling performed in this study for the 10-month dredging window are also described in Chapters 2 and 3.

## Sediment transport modeling

Two sediment transport models were used in this study: MPFATE and LTFATE. Background theory and formulation of these models are provided in Chapter 4.

MPFATE represents the accumulated sedimentation resulting from multiple placements from hoppers and scows. MPFATE is a Lagrangian model which represents dredged material descent from the placement vessel, collapse of the dredged material on the sediment bed, and passive transport of dredged material in suspension. MPFATE was applied to estimate initial conditions at the DMP sites following a season of DMP originating from the lower, middle, and inner harbor channels.

To improve on the MPFATE simulation of the formation of dredge material mounds from those generated in the previous GH modeling study, the following modifications were made to the version of MPFATE used in the study by Demirbilek et al. (2010): a) added capability for dredged material release from moving vessels; b) added capability for representing dredged material layers within hopper/barge (required for placement from moving vessels); c) added an option to output MPFATE results as source inputs for LTFATE; and d) modified the placement generation utility to layout placements for uniform lifts in rectangular placement sites. These changes enabled the first external coupling of MPFATE and LTFATE.

Clamshell-dredged sediments may not be completely broken apart by the dredging process. Fragments of the sediment bed (clumps) may be present within the barge and will settle rapidly to the bed during placement. Clump fraction depends upon dredging methods, sediment composition, sediment consolidation, and other factors. Therefore, there is a high degree of uncertainty in clump fraction. To bound the uncertainties in model simulations, clump fractions of 10 and 50 percent were applied in this study.

LTFATE is an Eulerian hydrodynamics and sediment transport model. The hydrodynamic and transport model in LTFATE is a finite difference model that solves the three-dimensional, vertically hydrostatic, free surface, turbulence averaged equations of motion. It contains dynamically linked hydrodynamic and constituent transport modules and can simulate barotropic and baroclinic flow in a water body due to astronomical tides,

wind, density gradients, and river inflow. SEDZLJ is the sediment transport model in LTFATE and solves for wave- and current-induced bed shear stresses, cohesive and noncohesive sediment erosion and deposition, bed-load transport of noncohesive sediment, bed armoring, consolidation of new deposits of fine-grain sediment, and morphologic changes resulting from erosion and deposition. The transport module in LTFATE is used to simulate the advective and dispersive transport of suspended sediment. LTFATE was applied to GH to estimate the erosion and subsequent transport and fate of O&M dredged material and channel deepening sediments placed at the two identified DMP sites for the two specified dredging scenarios.

The MPFATE and LTFATE models simulated three placement scenarios and two dredged material condition scenarios. The simulations indicated:

1. Potential navigation obstruction for the scenario with additional 2.0 MCY and highly clumped dredged material.
2. Potential navigation obstruction for the scenario with additional 1.0 MCY and highly clumped dredged material.
3. Channel obstructions were significantly reduced at the PCDS for Scenario 3 where the maximum channel obstruction was 170 ft for the 50 percent clump scenario.

## Recommendations

Based on the results obtained from the LTFATE modeling, the following two recommendations are made:

1. Scenario 3 is the preferred scenario as it produces a minimal obstruction to the navigation channel over the course of the placement and less channel sedimentation.
2. Modify the placement strategy at the SJDS by placing more material in the eastern half than in the western half of the site rather than the uniform placement strategy used at present.

# 1 Introduction

## 1.1 Background

The U.S. Army Engineer District, Seattle (NWS) makes management decisions regarding the most effective use of maintenance dredged material for the Federal Navigation Project at Grays Harbor (GH), Washington (Figure 1-1). The GH estuary is located in the southwest Pacific Ocean coast in the State of Washington about 50 miles north of the Columbia River mouth and approximately 150 miles south of the Strait of Juan de Fuca. Through a number of previous physical, numerical modeling, and field data collection efforts, the NWS has developed a large body of knowledge and data on Operations and Maintenance (O&M) of the navigation channel and impact of dredging operations on three Dredged Material Placement (DMP) sites in the inlet region. Figure 1-2 shows the locations of the three DMP sites – the Half Moon Bay Beneficial Use Site (HMBBUS), the Point Chehalis Disposal Site (PCDS), and the South Jetty Disposal Site (SJDS).

The GH complex is one of the largest estuaries in the United States. This estuary is long and elongated, and although it is mainly in a west-eastward direction, the navigation channel follows a zigzag pattern (Figure 1-3). The middle section of estuary is nearly 15 miles wide at its broadest point and, where the channel passes through it, is deeper than water areas north and south of the channel. It has a relatively large tidal range (~ 3 m) and one of the largest tidal prisms on the US Pacific Coast. Energetic incident waves of the Pacific Ocean and strong flood-ebb cyclic semi-diurnal tidally dominated flows are the main forces controlling the dynamic behavior of the GH navigation channel. The wide GH entrance is exposed directly to waves and tides of the Pacific Ocean. The eastern portion of the estuary is narrower and depths are relatively shallower compared to the open and relatively deep west side.

The north and south jetties at the entrance to GH were constructed between 1894 and 1916, and the shorelines both on the north and south sides of the entrance to GH have since experienced significant changes. The jetties were constructed to minimize the dredging requirements for the federal deep-draft navigation channel by training the tidal current that carries material from the entrance area to offshore depths. By 1915, the offshore beach profile steepened sharply and the initially accreted new

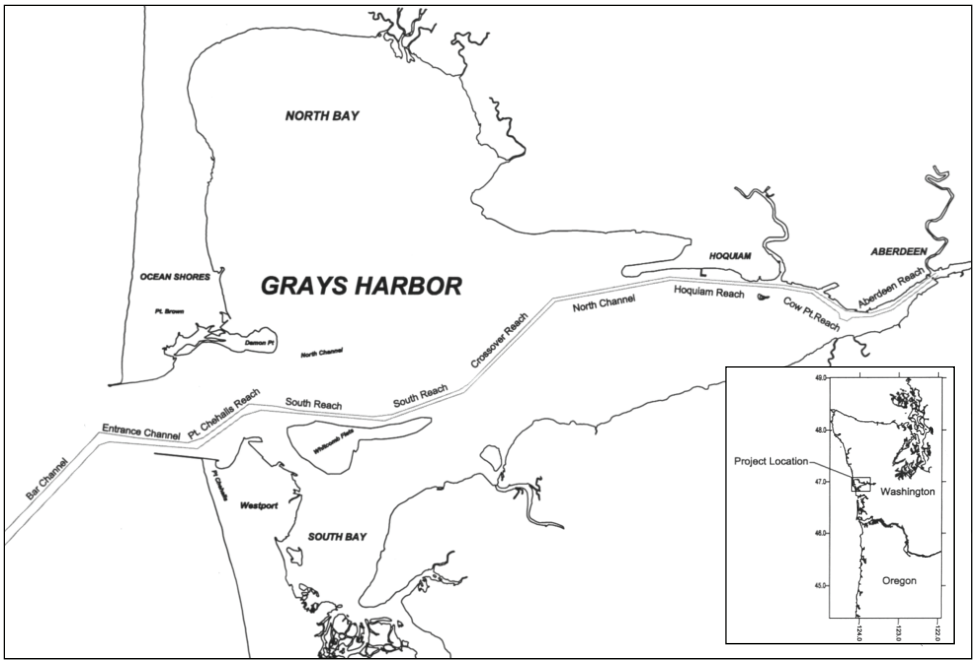


Figure 1-1. Grays Harbor navigation project and channel reaches.

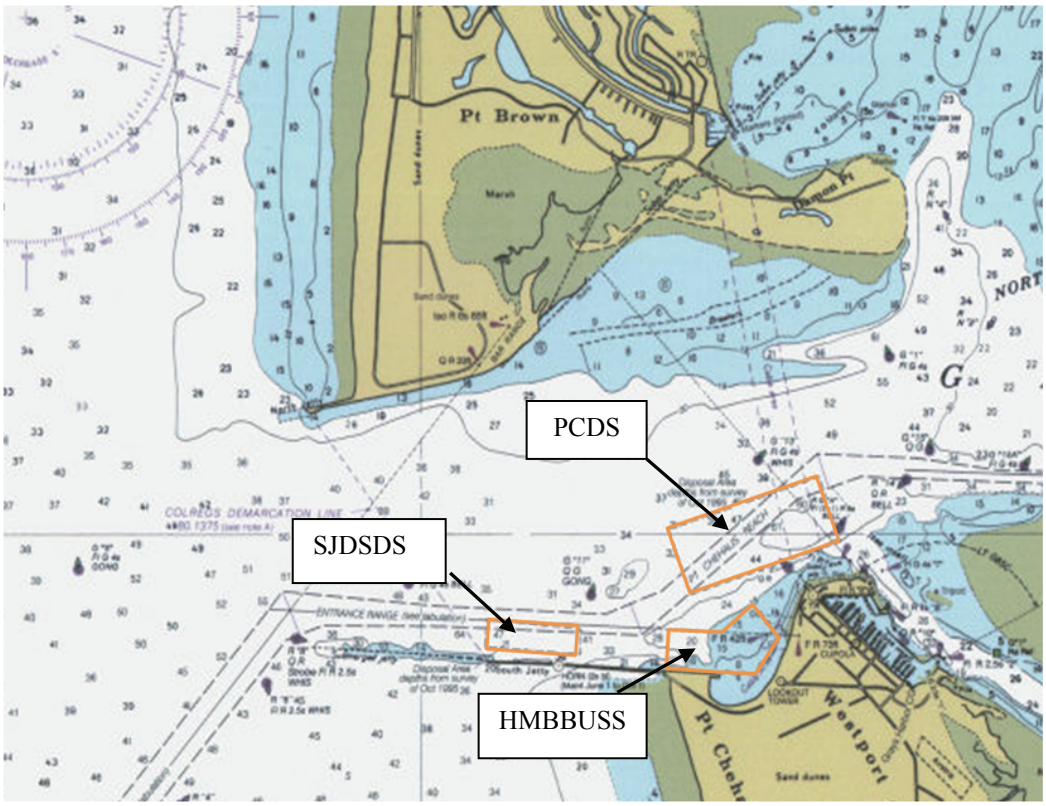


Figure 1-2. Dredged material placement sites (orange lines are the boundaries of the sites). HMBBUS – Half Moon Bay. PCDS – Point Chehalis. SJDS – South Jetty.

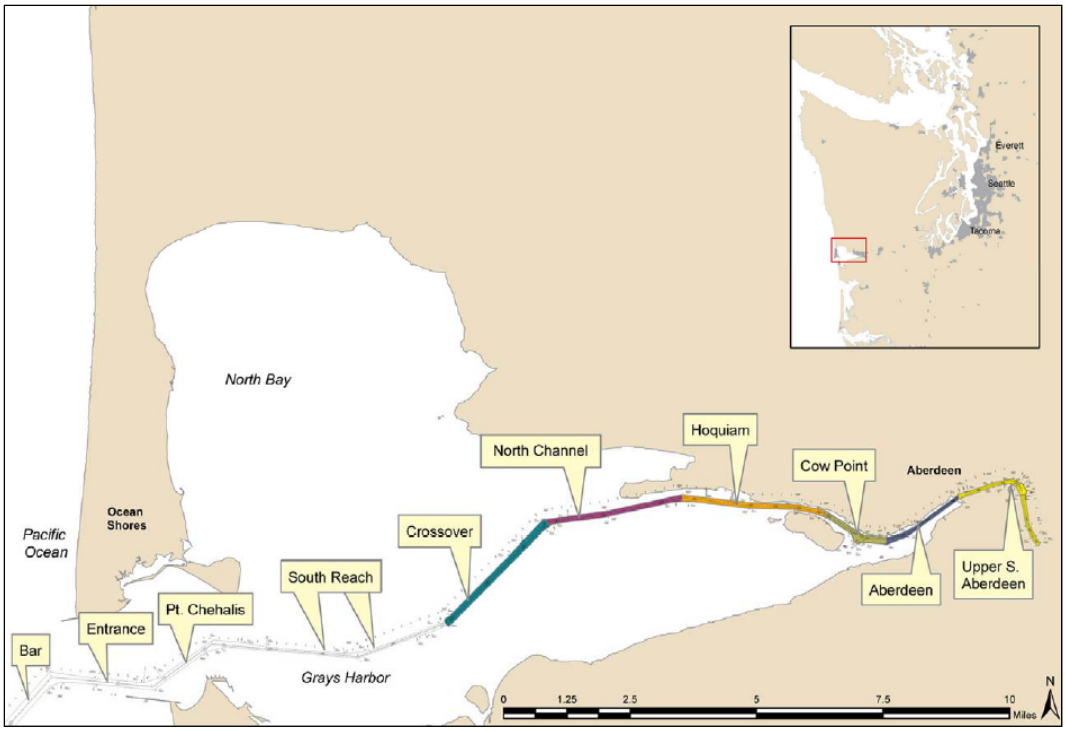


Figure 1-3. Grays Harbor navigation channel project reaches.

land seaward along the shoreline directly south of the South Jetty had begun to recede. In December 1993, the South Beach shoreline breached at the South Jetty root and the risk to navigation through the channel increased. The breach was filled in August 1994 with material dredged from the Federal navigation channel (Kraus et al. 2003).

The GH navigation channel transitions from the Pacific Ocean into the Point Chehalis Reach generally in a northeasterly direction, as shown in Figures 1-1 and 1-3. It enters the inlet in a northeasterly direction, and maintains an easterly direction in close proximity to the south jetty, turning abruptly northeast at Point Chehalis Reach. The sediment characteristics of the reaches vary, with sand being dominant westward of the South Reach, and mud (mixture of gravels, fine sand, silt and clay) becoming increasingly dominant in the reaches eastward of South Reach. Maintenance dredging requirements for the Point Chehalis and Cow Point reaches have been the most excessive. Consequently, past field measurements by the NWS were directed to collection of wave and current data, and evaluation of alternate channel orientations and depths to determine the optimal channel design for minimizing maintenance dredging requirements.

As stated previously, the NWS has established three DMP sites inside the GH estuary for management of the dredged material extracted from the navigation channel. The PCDS was established in 1976. The SJDS feeds the scour area adjacent to the south jetty trunk, and began receiving dredge material in 1988. The third site is the nearshore HMBBUS that was established in 1992 to slow erosion of the HMB shoreline. The inner harbor sediments (silts/clays) are currently placed exclusively at the PCDS and the SJDS, while the outer harbor sediments (>95 percent marine sand) are placed at three interior and other open-water disposal sites. Periodic annual dredging operations are conducted to maintain the authorized depth in the channel reaches for efficiency and safety of deep-draft water transportation in the GH estuary. Clamshell and hopper dredges are used in the annual maintenance dredging operations. The dredged material is placed at existing open-water disposal sites and nearshore beneficial use placement sites. The beneficial usage of dredge material ensures that the Point Chehalis revetment extension remains buried and helps to maintain a stable, sandy beach profile of HMB. Beach nourishment is applied on South Beach and the eastern shore of HMB to minimize the risk of jetty flanking and a future breach from occurring adjacent to the south jetty. The rest of the dredged material is placed at the PCDS, SJDS, or South Beach Beneficial Use Site located in the nearshore region south of the south jetty in the Pacific Ocean.

NWS recently evaluated the GH navigation channel realignment in the Point Chehalis/Entrance reach because historic trends in survey data indicated that this area was naturally scouring a new thalweg just north of the present channel. The realigned channel would take advantage of the thalweg, and a relocated channel was hypothesized to reduce annual dredging quantities. The impact of DMP sites on channel maintenance was also examined. The key issues of interest to the NWS that were investigated in that study performed by Demirbilek et al. (2010) were: a) changes in waves and hydrodynamics at GH navigation channel over time scales of 0.5 to 5 years, b) consequences of channel realignment on waves, hydrodynamics and sedimentation of GH navigation channel, c) sediment transport pathways in the lower GH and at three DMP sites, and d) channel infilling estimates from frequently occurring, low energy storms and less frequent, but more energetic storms. These issues were examined for two channel alternatives: “Existing” and “Realigned” channel configurations. The 2010 study utilized wave and hydrodynamic modeling results from CMS-Wave and ADCIRC models for the existing and realigned channels to

drive the MPFATE, GTRAN, and LTFATE sediment transport models that were used to simulate both short- and long-term sediment transport at GH. The findings from that study included the following: 1) very little placed sediment eroded from the PCDS for the realigned channel configuration; 2) the residence times were less at the SJDS than at the PCDS.

In FY 2011 the NWS requested that the U.S. Army Engineer Research and Development Center (ERDC), Coastal and Hydraulics Laboratory (CHL) perform a companion or follow-up numerical modeling study for the purpose of performing a DMP site capacity analysis for two of the three DMP sites for a Navigation Improvement Project. The specific goal of this study is to estimate the short-term and long term fate of channel deepening sediments as well as the annual O&M dredge material placed at the two DMP sites in the entrance channel to GH.

## 1.2 Present study plan

The objective of the present modeling study is to calculate both the short term and long-term fate of channel deepening sediments dredged from the South Reach, Crossover Reach, North Reach, Hoquiam Reach, and Cow Point Reach reaches and placed at the SJDS and the PCDS. Specifically, the following three disposal scenarios will be simulated: placement of an additional 1) 2.0 million cubic yards (MCY), 2) 1.0 MCY, and 3) 2.0 million cubic yards (MCY) of dredged material from the South Reach, Crossover Reach, North Reach, Hoquiam Reach, and Cow Point Reach in addition to the annual O&M dredging material placed at the two sites. For the third scenario the PCDS was moved to the north 1000 ft (305 m) and the area designated for dredged material placement was the full site (5000 ft (1524 m) long and 2000 ft (610 m) wide).

The following tasks were used to accomplish the stated objective for the Navigation Improvement Project:

1. Using the existing ADCIRC model of GH (see Demirbilek et al. 2010), the specified 10-month dredging window (April 15, 2006 to February 14, 2007) will be simulated for the site capacity analysis of the two DMP sites.
2. The output from the 10-month ADCIRC model run will be used to construct the tidal forcing boundary conditions for the ocean boundaries in the existing LTFATE model of GH (see Demirbilek et al. 2010).
3. Initially, the plan was to perform only tidal current induced sediment transport at the two DMPs. The importance of including wave-induced bed

shear stresses in the LTFATE simulations was evaluated by comparing bed shear stresses calculated with and without waves at the SJDS over the period July 15 – September 30. The result from this comparison (discussed in more depth in Chapter 5) indicated that waves contribute significantly to the peak bed shear stresses. Therefore, the decision was made to perform wave modeling using the existing GH CMS-Wave model for the 10-month dredging window so that both tide- and wave-induced sediment transport modeling could be performed using LTFATE.

4. To improve the MPFATE simulation of the formation of dredge material mounds from those generated in the previous GH modeling study, the following modifications were made to the version of MPFATE used in the study by Demirbilek et al. (2010): a) add capability for representing dredged material layers within hopper/barge; b) include capability for dredged material release from moving vessels; c) add option to output MPFATE results as source inputs for LTFATE; and d) modify the placement generation utility to layout placements for uniform lifts in rectangular placement sites. These changes enabled the first external coupling of MPFATE and LTFATE to be made.
5. Perform MPFATE modeling for the two placement scenarios over the 10-month dredging window. The details of this modeling and how the external coupling to LTFATE was utilized will be explained in detail in Chapter 5.
6. Perform LTFATE modeling for the three placement scenarios over the 10-month dredging window. The details of this modeling and how the external coupling to MPFATE was utilized will be explained in detail in Chapter 5.
7. Analysis and interpretation results from the numerical modeling performed in Tasks 5 and 6.

This report is organized as follows. The wave and hydrodynamic models used in this study (CMS-Wave and ADCIRC, respectively) are described in Chapter 2, and their applications to GH are described in Chapter 3. The two sediment transport models used in this study (MPFATE and LTFATE) are described in Chapter 4. The methodology used in application of MPFATE and LTFATE to simulate the formation of dredge material placement mounds and their subsequent erosion is described in Chapter 5. The results obtained from the 10-month long simulations of the three dredging scenarios using LTFATE are described in Chapter 6. Conclusions and recommendations from this modeling study are provided in Chapter 7.

# 2 Description of Wave and Hydrodynamic Models

## 2.1 Wave model

The spectral wave model CMS-Wave is used in this study to compute wave transformation from offshore to nearshore. It is based on the wave-action balance equation that includes wave refraction, shoaling, diffraction, reflection, breaking, and dissipation. It is a two-dimensional spectral wave model formulated from a parabolic approximation equation (Mase et al. 2005a; 2005b) with energy dissipation and diffraction terms to simulate a steady-state spectral transformation of directional random waves co-existing with ambient currents in the coastal zone. The model operates in full-plane mode, but was applied in this large-domain study for numerical efficiency to a coastal half-plane for waves propagating only from the seaward boundary toward shore. Wave generation (wind input), wave refraction, shoaling, diffraction and reflection, wave breaking, bottom friction, and wave dissipation are considered in this model. The model technical reports ERDC/CHL TR-08-13 (Lin et al. 2008) and ERDC/CHL TR-11-10 (Lin et al. 2011) provide CMS-Wave verification and validation and examples (Demirbilek and Rosati 2011) to demonstrate model's applicability to propagation of random waves over complicated nearshore bathymetry where wave refraction, diffraction, reflection, shoaling, and breaking occur simultaneously. The report describes model's general features, formulation, capabilities, input and output, and provides application guidelines.

The height and direction of waves approaching GH Navigation channel change due to wave shoaling, refraction, diffraction, reflection, and breaking. Waves propagating through the GH channel interact with the bathymetry and are affected by surrounding land features, and currents and coastal structures. Advanced linear and nonlinear wave theories and solution methods may be used in wave transformation models for mono-chromatic and irregular or random waves moving from deep to shallow waters over varying bathymetry (Nwogu and Demirbilek 2001; Demirbilek and Panchang 1998). Each wave theory and associated numerical model has certain advantages and limitations, and appropriateness of the models depends on the relative importance of various physical processes and the

particular requirements of a project. A spectral wave model was necessary for this project given the large extent of modeling domain over which wave estimates were required.

By definition, CMS-Wave spectral model transforms a wave spectrum of natural sea waves that is considered as the sum of a large number of harmonic waves, each with constant amplitude and phase, randomly chosen for each observance of a true record (Demirbilek and Vincent 2010). The CMS-Wave transformation model selected for GH navigation project represents irregular wave forms and provides estimate of wave parameters necessary for flow and sediment transport models.

CMS-Wave incorporates wind-wave generation, bottom friction, and spatially varied cell sizes that make model suitable for more general use in the coastal region. Wave diffraction is included in the governing equations following the method of Mase et al. (2005a). Four different depth-limiting wave breaking formulas are provided including one for the wave-current interaction based on the dispersion relationship for wave blocking by an opposing current. Wave generation and whitecapping dissipation are based are parameterized as a source term and calibrated using field data (Lin and Lin 2004a and b, 2006). Bottom friction loss is estimated based on the classical drag law formula (Collins 1972). Other features in CMS-Wave include grid nesting capability, variable rectangular cells, wave overtopping, wave runup on beach face, and wave-wave interaction.

The governing equation of CMS-Wave is the wave-action balance equation given by (Mase 2001):

$$\frac{\partial\left(C_x N\right)}{\partial x}+\frac{\partial\left(C_y N\right)}{\partial y}+\frac{\partial\left(C_\theta N\right)}{\partial \theta}=\frac{\kappa}{2\sigma}\left[\left(CC_g \cos^2\theta N_y\right)_y-\frac{CC_g}{2}\cos^2\theta N_{yy}\right]-\varepsilon_b N-S \quad (2\text{-}1)$$

where

$$N=\frac{E(\sigma,\theta)}{\sigma} \quad (2\text{-}2)$$

is the wave-action density to be solved and is a function of frequency $\sigma$ and direction $\theta$. $E(\sigma,\theta)$ is spectral wave density representing the wave energy per unit water-surface area per frequency interval. We note that in the presence of an ambient current, the wave-action density is conserved, whereas the

spectral wave density is not (Bretherton and Garrett 1968; Whitham 1974). Both wave diffraction and energy dissipation are included in the governing equation. The implementation of the numerical scheme is described elsewhere (Lin et al. 2008; Mase et al. 2005a; Mase 2001). $C$ and $C_g$ are wave celerity and group velocity, respectively; $x$ and $y$ are the horizontal coordinates; $C_x$, $C_y$, and $C_\theta$ are the characteristic velocity with respect to $x$, $y$, and, $\theta$ respectively; $N_y$ and $N_{yy}$ denote the first and second derivatives of $N$ with respect to $y$, respectively; $\kappa$ is an empirical parameter representing the intensity of diffraction effect; $\varepsilon_b$ is the parameterization of wave breaking energy dissipation; $S$ denotes additional source $S_{in}$ and sink $S_{ds}$ (e.g., wind forcing, bottom friction loss, etc.) and nonlinear wave-wave interaction term. The treatment of wave diffraction, wave reflection, wave breaking, wave-current interaction, wind forcing, and whitecapping dissipation are described in the model's technical report (Lin et al. 2008). For additional information about the most recent CMS-Wave capabilities, interested readers should consult Lin et al. (2011) and Demirbilek and Rosati (2011).

## 2.2 Hydrodynamic model

The two-dimensional, depth-integrated implementation of the ADvanced CIRCulation (ADCIRC-2DDI) model was used in the present study. The ADCIRC-2DDI model was implemented to calculate water-surface elevations and depth-averaged currents in the GH study area. ADCIRC is a well-established computer model that for solves for the time dependent free surface and current fields using the nonlinear shallow-water equations (NSWEs) in two horizontal dimensions. It utilizes the finite element method in space and therefore can be run on highly flexible, irregularly spaced grids. Fine resolution can be specified in the area of interest and coarse resolution can be specified in areas distant from the region of interest. Model accuracy is directly related to the ability to resolve bathymetric features such as navigation channels, dredge mounds, structures (jetties and breakwaters), shorelines and topographic features, and ADCIRC's unstructured grid system allows this to be done well.

Additional factors considered in the selection of the flow model were: ADCIRC is a fully nonlinear finite element model that is capable of simulating two-dimensional shallow water equations. It provides forcing to other USACE hydrodynamic models that calculate sediment transport that is coupled to bed and hydrodynamic changes. The ability of ADCIRC to allow the domain to wet and dry as the tide changes is suitable for the shallow coastal environment.

Many publications, external reports, and journal papers provide in-depth information about theory, numerical features and performance of ADCIRC in numerous research studies and practical applications. Thus, only a summary of the governing equations is provided here. More details of the two-dimensional shallow water equations and its computational philosophy and equations can be found in http://www.adcirc.org/.

The ADCIRC-2DDI is the two-dimensional, depth-integrated implementation of the ADCIRC coastal ocean model (Luettich et al. 1992; Westerink et al. 1992; Westerink et al. 1993; Luettich and Westerink 2004). It is used in this study to perform the hydrodynamic computations. Imposing the wind and atmospheric pressure fields, the ADCIRC model can replicate tide induced and storm-surge water levels and currents. In two dimensions, the model is formulated with the depth-averaged shallow water equations for conservation of mass and momentum. Furthermore, the formulation assumes that the water is incompressible, hydrostatic pressure conditions exist, and that the Boussinesq approximation is valid. Using the standard quadratic parameterization for bottom stress and neglecting baroclinic terms and lateral diffusion effects, the following set of conservation equations in primitive, nonconservative form, and expressed in a spherical coordinate system, are incorporated in the model (Flather 1988; Kolar et al. 1993):

$$\frac{\partial U}{\partial t}+\frac{1}{r\cos\phi}U\frac{\partial U}{\partial \lambda}+\frac{1}{R}V\frac{\partial U}{\partial \phi}-\left[\frac{\tan\phi}{R}U+f\right]V= -\frac{1}{R\cos\phi}\frac{\partial}{\partial \lambda}\left[\frac{p_s}{\rho_o}+g(\zeta-\eta)\right]+\frac{\tau_{s\lambda}}{\rho_o H}-\tau_* U \tag{2-3}$$

$$\frac{\partial V}{\partial t}+\frac{1}{r\cos\phi}U\frac{\partial V}{\partial \lambda}+\frac{1}{R}V\frac{\partial V}{\partial \phi}-\left[\frac{\tan\phi}{R}U+f\right]U= -\frac{1}{R}\frac{\partial}{\partial \phi}\left[\frac{p_s}{\rho_o}+g(\zeta-\eta)\right]+\frac{\tau_{s\lambda}}{\rho_o H}-\tau_* V \tag{2-4}$$

$$\frac{\partial \zeta}{\partial t}+\frac{1}{R\cos\phi}\left[\frac{\partial UH}{\partial \lambda}+\frac{\partial (UV\cos\phi}{\partial \phi}\right]=0 \tag{2-5}$$

where $t$ = time; $\lambda$ and $\varphi$ = degrees longitude (east of Greenwich is taken positive) and degrees latitude (north of the equator is taken positive); $\zeta$ = free surface elevation relative to the geoid, $U$ and $V$ = depth-averaged

horizontal velocities in the longitudinal and latitudinal directions, respectively; $R$ = the radius of the earth; $H = \zeta + h$ = total water column depth; $h$ = bathymetric depth relative to the geoid; $f = 2\Omega \sin \varphi$ = Coriolis parameter; $\Omega$ = angular speed of the earth; $p_s$ = atmospheric pressure at free surface; $g$ = acceleration due to gravity; $\eta$ = effective Newtonian equilibrium tide-generating potential parameter; $\rho_o$ = reference density of water; $\tau_{s\lambda}$ and $\tau_{s\varphi}$ = applied free surface stresses in the longitudinal and latitudinal directions, respectively; and $\tau$ = bottom shear stress and is given by the expression $C_f (U^2 + V^2)^{1/2} / H$ where $C_f$ is the bottom friction coefficient.

The momentum equations (Equations 2-3 and 2-4) are differentiated with respect to $\lambda$ and $\tau$ and substituted into the time differentiated continuity equation (Equation 2-5) to develop the following Generalized Wave Continuity Equation (GWCE):

$$\frac{\partial^2 \zeta}{\partial t^2} + \tau_o \frac{\partial \zeta}{\partial t} - \frac{1}{R\cos\phi}\frac{\partial}{\partial \lambda}\left[\frac{1}{R\cos\phi}\left(\frac{\partial HUU}{\partial \lambda} + \frac{\partial (HUV\cos\phi)}{\partial \phi}\right) - UVH\frac{\tan\phi}{R}\right] -$$
$$2\omega \sin\phi\, HV + \frac{H}{R\cos\phi}\frac{\partial}{\partial \lambda}\left(g(\zeta - \alpha\eta) + \frac{p_s}{[}p_o\right) + \tau_* HU - \tau_o HU - \tau_{s\lambda} -$$
$$\frac{1}{R}\frac{\partial}{\partial \phi}\left[\frac{1}{R\cos\phi}\left(\frac{\partial HVV}{\partial \lambda} + \frac{\partial HVV\cos\phi}{\partial \phi}\right) + UUH\frac{\tan\phi}{R} + 2\omega\sin\phi\, HU\right] + \quad (2\text{-}6)$$
$$\frac{H}{R}\frac{\partial}{\partial \phi}\left(g(\zeta - alfa\eta) + \frac{p_s}{\rho_o}\right) + \tau_* - \tau_o HV - \frac{\tau_{s\lambda}}{\rho_o}] -$$
$$\frac{\partial}{\partial t}[\frac{VH}{R}\tan\phi\,] - \tau_o[\frac{VH}{R}\tan\phi] = o$$

The ADCIRC model solves the GWCE in conjunction with the primitive momentum equations given in Equations 2-3 and 2-4. The GWCE-based solution scheme eliminates several problems associated with finite-element programs that solve the primitive forms of the continuity and momentum equations, including spurious modes of oscillation and artificial damping of the tidal signal. Forcing functions include time-varying water-surface elevations, wind shear stresses, and atmospheric pressure gradients.

The ADCIRC model uses a finite-element algorithm in solving the governing equations over complicated bathymetry encompassed by irregular sea/shore boundaries. This algorithm allows for extremely flexible spatial discretizations over the entire computational domain and has demonstrated

excellent stability characteristics. The advantage of this flexibility in developing a computational grid is that larger elements can be used in open-ocean regions where less resolution is needed, whereas smaller elements can be applied in the nearshore and estuary areas where finer resolution is required to resolve hydrodynamic details.

# 3 Hydrodynamic and Wave Modeling

## 3.1 Bathymetric data

Bathymetric data collected by the NWS in 1999, 2003, and 2008 were used in verification of flow and wave models to develop hydrodynamic and wave input conditions for sediment transport models. Depths on the numerical model grids were referenced to Mean Tide Level (MTL). Figure 3-1 shows the variation of depth in the region from deepwater to offshore bar, and to the entrance channel and bay. Figure 3-2 provides bathymetric contours depicting depth change along the navigation channel and in eastern end of estuary. The channel bathymetry for the model runs performed in this study was collected by the NWS in 2011 and used to update the MPFATE and LTFATE model grids.

## 3.2 Hydrodynamic modeling

ADCIRC (Demirbilek et al. 2010) was used in the hydrodynamic modeling. The ADCIRC model domain is shown in Figure 3-3. As seen, the ADCIRC domain and geometric/topographic description and resulting computational grid covers the shallow areas of GH surrounded by land, where water depths vary from 0 m to 16 m. The model domain extends seaward to depths of thousand of meters in the deep Pacific Ocean. The model domain boundaries were selected to ensure for the correct development, propagation, and attenuation of tides and storms without necessitating nested solutions or specifying ad hoc boundary conditions for tides or storm surge. The domain has a 1,250 miles (2,000 km) open-water boundary (Figure 3-3). The extent of the domain was confined in a geographic range defined by longitude of 130.5 deg to 122.7 deg W and latitude of 40.7 deg to 51.2 deg N. Its open ocean boundary is located in the deep ocean that lies outside the resonant basins, and is not located near the tidal amphidromes. Developing the ADCIRC mesh involved a) defining domain extent, b) preparing bathymetric data, c) assigning depth values to shoreline, c) referencing the bathymetric data to the model datum, and d) defining tidal flats within the GH estuary.

The area of interest in this project extends to approximately the 20 m depth contour to the West of the Entrance Channel, 13 km north of the North Jetty and 9 km south of the South Jetty. The varying resolution was added so that

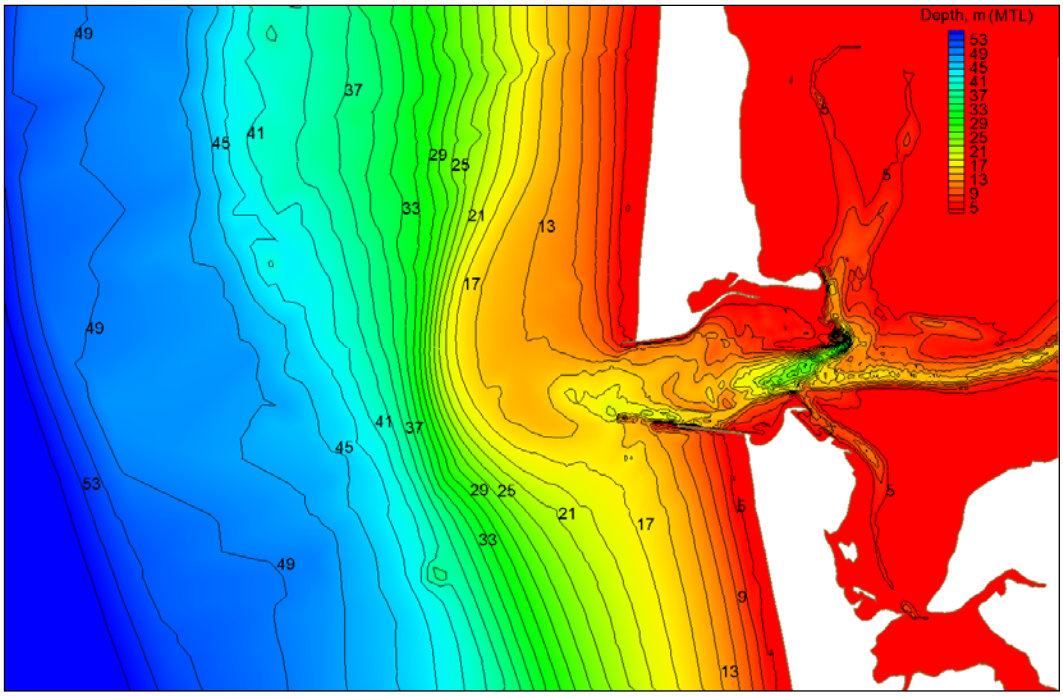


Figure 3-1. Depth contours at Grays Harbor between offshore and entrance channel.

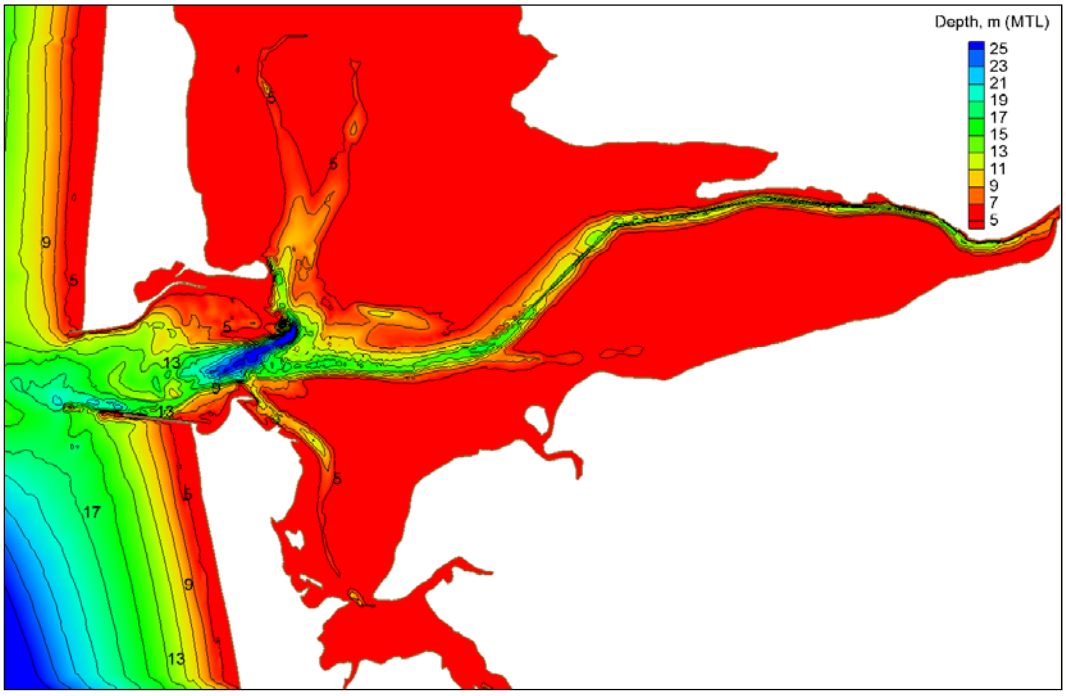


Figure 3-2. Depth contours inside the Grays Harbor estuary.

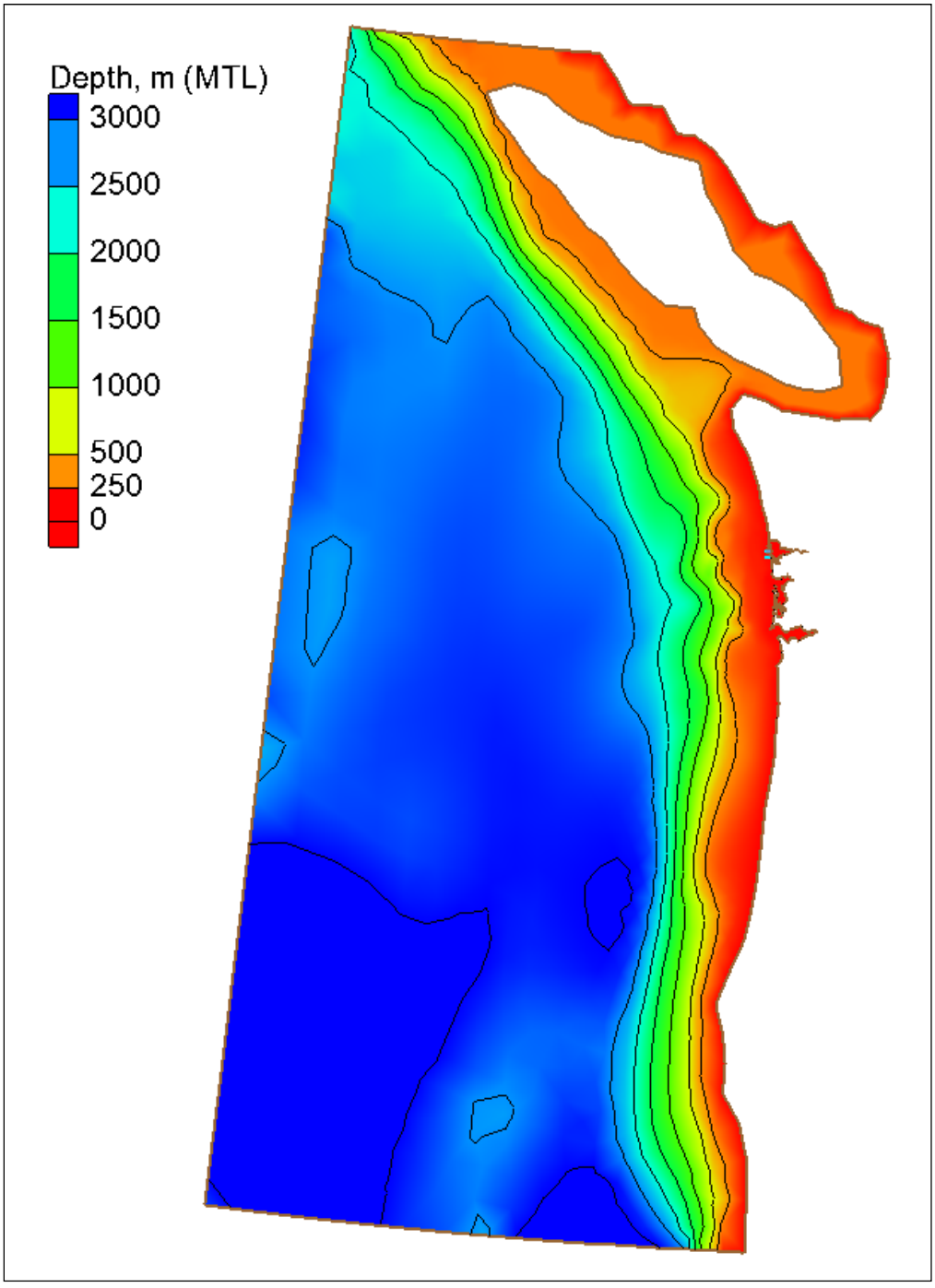


Figure 3-3. Regional ADCIRC model domain.

the navigation channel is at the smallest resolution. The development of an accurate unstructured mesh for circulation modeling at GH requires appropriate selection of model domain and optimal resolution of features affecting propagation of tide and wind induced flow.

The tidal response at the model domain's open boundary is dominated by the astronomical constituents and nonlinear energy is limited due to the depth. The storm surge response along this boundary is essentially an inverted barometer pressure effect directly correlated to the atmospheric pressure deficit in the meteorological forcing; and it can therefore be easily specified. This boundary allows the model to accurately capture basin-to-shelf physics. The mesh design provides localized refinement of the coastal areas of GH estuary and of the important hydraulic features. Attention was focused on the level of detail of the navigation channel, and areas near the SJDS and PCDS, with nodal spacing reaching as low as 10 m in the most highly refined areas. This unstructured mesh can resolve the critical features and the associated local flow processes with orders of magnitude fewer computational nodes because it provides resolution on a localized basis and fine resolution generally extends far outside the necessary area.

The ADCIRC mesh for GH contains approximately 40,000 nodes and 77,000 elements. Mesh resolution varies from 50 km in the deep Pacific Ocean to about 50 m in the GH estuary complex. The dense mesh resolution required for the study region leads to a final mesh with more than 85 percent of the computational nodes placed within the estuary, starting at the outer bar of Navigation channel outside the entrance. This enabled sufficient resolution while minimizing the computational run time for such an extensive domain. Geometry, topography and bathymetry in the GH mesh were all defined in coordination with the NWS. The bathymetry data provided by the NWS included the most recent surveys conducted following maintenance dredging of the navigation channel and replicated the prevailing conditions in 2008. The bathymetric and topographic data were interpolated to the GH computational mesh by moving progressively from the coarsest and deepest to finest and shallowest areas of the computational domain. Bathymetric contours between the outer bar and entrance channel area were further revised based on recent data by the NWS, obtained from ongoing studies by NOAA, USGS, and tsunami research community works for the Northwest Pacific Ocean region.

Element areas vary greatly in the GH mesh, with the ratio of the offshore element to the smallest element in the navigation channel area being 1,000. Mesh resolution can vary spatially, and grading between coarse and fine resolution was done with regard to transition between element areas. A general rule is that adjacent elements should not differ in size by more than 50 percent. More resolution was added to the study area as shown in

Figure 3-4 with finest node spacing of about 10 m near the South Jetty, along the channel and at the Point Chehalis.

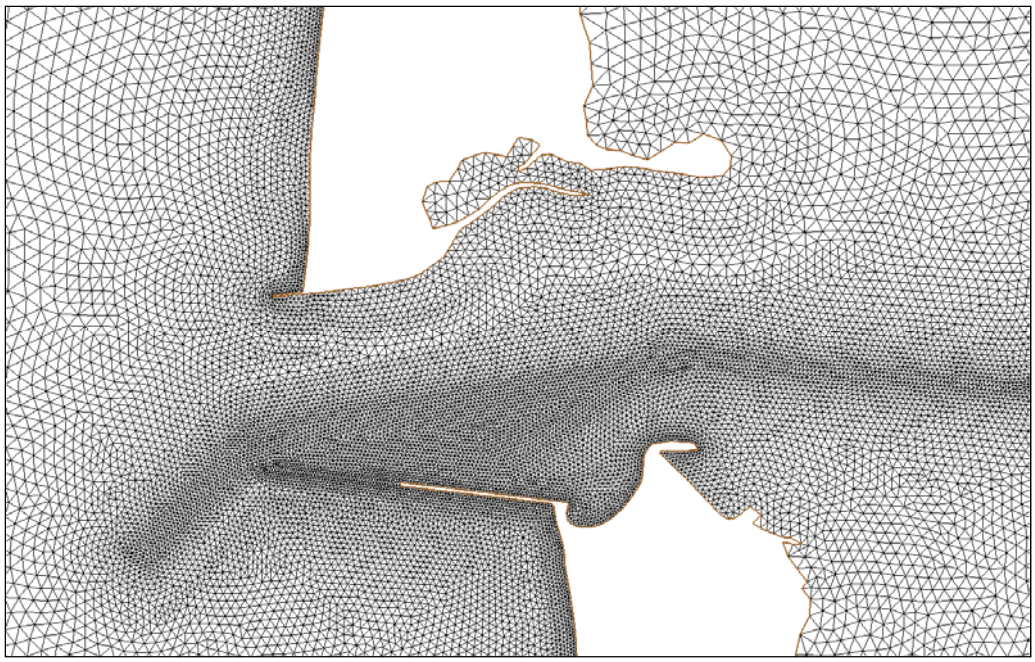

Figure 3-4. ADCIRC mesh at the Grays Harbor entrance.

Hydrodynamic forcing of the study area included forcing with a time series of water level forcing constructed from astronomical tidal constituents at the open ocean boundary. The model was run with the Le Provost tidal constituent database (Le Provost et al. 1994). This tidal constituent database was selected to force the model because it produced better agreement between the model water surface values and the measured tide gauges in the region.

Wind and tide forcings were included in the circulation model runs. River flow influxes are not considered since the emphasis in this study is on the sediment issues at the outer navigation channel caused by tides and waves. Meteorological forcing of surface wind and atmospheric pressure defined on a longitude, latitude grid, was interpolated in space onto the ADCIRC mesh. Wind data at 10-m elevation and water surface pressure were read every six hours from NCEP/NCAR Reanalysis data sets by Earth System Research Laboratory, NOAA (http://www.esrl.noaa.gov/psd/data/gridded/data.ncep.reanalysis.html).

The study also involved acquiring an extensive set of measured water level and current data in 1999 and 2003. An analysis of these data was undertaken to examine the water elevation fluctuations and magnitude and

directional characteristics of the current. These data were used to evaluate the accuracy of model results.

The 10-month simulation period for this project was split into five runs. These subset runs covered the following times:

- 2006 Q2 (4/15 – 7/3)
- 2006 Q3 (7/1 – 9/3)
- 2006 Q4a (9/1 – 11/3)
- 2006 Q4b (11/3 – 12/31)
- 2007 Q1 (1/1 – 2/28)

The reason for splitting up the simulations as shown above was to avoid queuing times and speed up runs on super-computers. Longer simulations would require a large number of processors and longer waiting in the run queues. Model results (surface elevation, and u- and v-velocities) were saved at hourly intervals at all ADCIRC mesh nodes. These results were used to construct the ocean boundary conditions for the LTFATE model that is described in the next chapter.

## 3.3 Wave modeling

The model domain of CMS-Wave and changes in depth contours are shown in Figure 3-5. The model computational domain covers approximately 330 square miles (860 square kilometers).

The non-uniform Cartesian finite-difference CMS-Wave model grid for GH is shown in Figure 3-6. As seen, it is oriented East-West, with the offshore boundary at 40 m depth contour, and extends eastward to Aberdeen, WA. The CMS-Wave model has 94,000 cells (68,000 computational cells and 26,000 non-computational cells) with the largest and smallest cell sizes of 2,000 m and 30 m, respectively. A variable grid was used in the areas from the entrance channel to Point Chehalis.

The same 10-month simulation period was split into five runs. These subset runs covered the following times:

- 2006 Q2 (4/15 – 7/3)
- 2006 Q3 (7/1 – 9/3)
- 2006 Q4a (9/1 – 11/3)
- 2006 Q4b (11/3 – 12/31)
- 2007 Q1 (1/1 – 2/28)

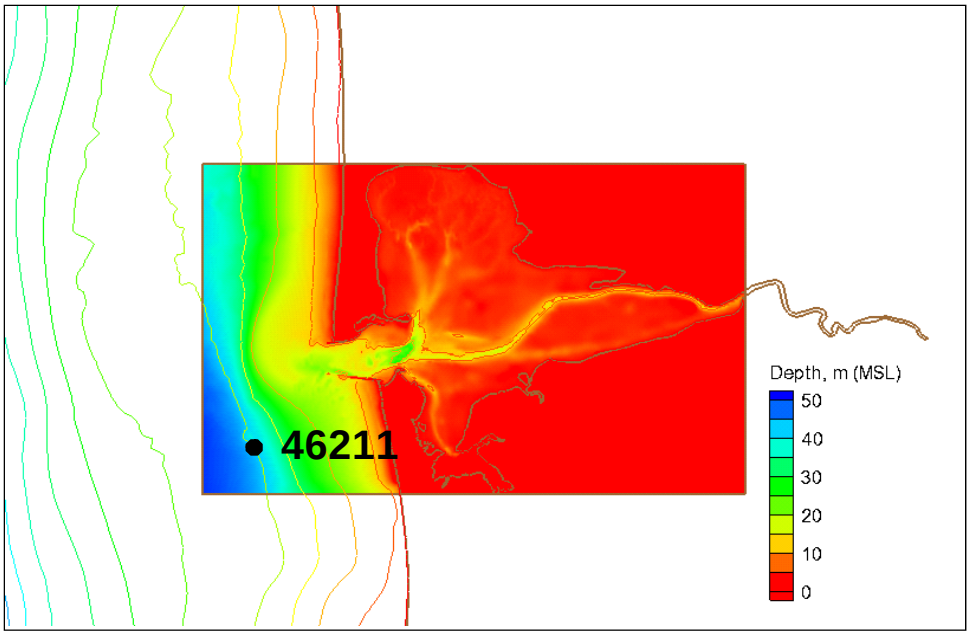


Figure 3-5. Model domain for the Grays Harbor CMS-Wave model.

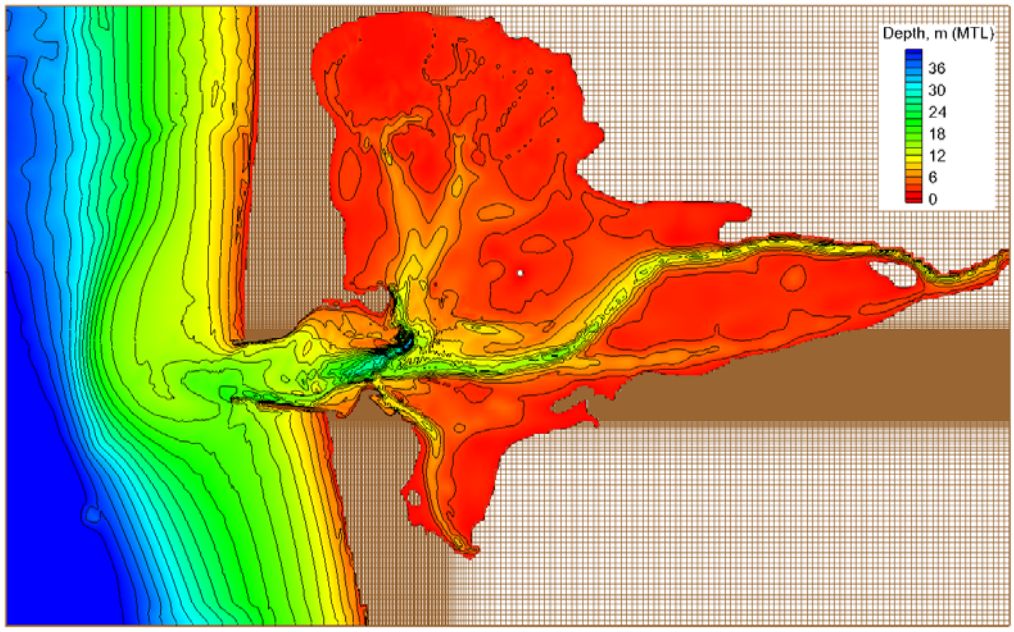


Figure 3-6. Non-uniform Cartesian CMS-Wave grid showing bathymetric changes.

The CMS-Wave simulation is forced by the regional ADCIRC water levels and currents, surface wind field, and offshore waves based on the CDIP Buoy 036 (NDBC 46211). Wave modeling results include waves and water levels at 3-hr intervals. Model solution files include the simulated wave heights, periods, and propagation directions. These temporally and spatially varying wave parameters were used to calculate the wave-induced bed shear stresses in LTFATE.

# 4 Description of Sediment Transport Models

## 4.1 Introduction

As stated previously, the objective of this modeling study is to calculate both the short term and long-term fate of channel deepening sediments dredged from the South Reach, Crossover Reach, North Reach, Hoquiam Reach, and Cow Point Reach reaches and placed at the SJDS and the PCDS. To accomplish this objective, two sediment transport models were applied. MPFATE was applied to estimate post-placement dredged material configurations within placement sites. LTFATE was applied to simulate the fate of mixed (sand and cohesive sediment) dredged material eroded and transported from two existing DMP sites. This chapter contains a description of these sediment transport models.

## 4.2 MPFATE

One goal of this study is to determine the bed structure following DMP at the Point Chehalis and South Jetty placement sites to define initial bed conditions for LTFATE simulations. The MPFATE model was configured and applied to DMP at the Grays Harbor disposal sites. Currents at the site were obtained from the ADCIRC (depth-averaged) hydrodynamic simulations described in Chapter 3. Dredged material placement was represented by convective descent, dynamic collapse, and suspended sediment transport processes. Dredged material characteristics and dredge vessel dimensions and operating parameters were developed from historical dredging records and sampling provided by NWS. Results of the simulations included post-dredge bathymetry at each placement site as well as lift heights. This section describes the sediment processes during dredging in Grays Harbor, how MPFATE represents these processes, and boundary conditions and input for MPFATE simulations.

### 4.2.1 Sediment processes during DMP operations

Dredged material placement operations with bottom-release scows and hopper dredges involves transport of dredged material from the dredging site to the placement site, positioning of the vessel at the point of release, and release of the dredged material through the bottom of the scow or

hopper. Frequency of placement at a DMP site is defined by the dredge production rate at the dredging site, capacity of the scow or hopper, and in the case of hopper dredges, the transit time between the dredging and placement sites.

Once released, the dredged material enters the water column as a dense fluid plume, descending through the water column through negative buoyancy. The point of impact of this dense, dredged-material plume on the bottom is governed by the velocity of the scow or hopper at time of release, the ambient currents, size and density anomaly of the plume, and water depth. Upon impact on the bottom, the dredged material vertical momentum is transferred to horizontal momentum and the plume spreads horizontally along the bottom until friction, viscosity, radial spreading, and sediment deposition arrest its horizontal movement.

### 4.2.2 Model description

MPFATE is intended to represent the dominant physical processes describing DMP site morphology throughout a dredging cycle (timescales of weeks to years). This model performs multiple functions representing the placement sequence, type of dredging equipment and sediment properties, physical processes during and immediately following placement (descent, collapse, passive transport), and physical processes at longer timescales following placement (consolidation, sediment transport, and avalanching). MPFATE model functions can be generally grouped into distinct components, each representing a defined process or group of processes influencing the ultimate morphology of a dredged material mound. Components of the model include: environmental conditions, dredged material description, definition of placement sequence, short-term physical processes, and long-term physical processes.

MPFATE simulations generally proceed with the user defining dredged material characteristics, environmental conditions (waves, currents, water level), scow or hopper dimensions and characteristics, and DMP operations (including vessel speed and location of placement for each load). MPFATE then develops the appropriate inputs for STFATE (Johnson 1990; Johnson and Fong 1995) for each hopper or scow load, including collection of appropriate environmental conditions (from hydrodynamic and wave models) and hopper/scow release locations. Short-term processes of DMP including convective descent, collapse, and passive dispersion are represented by STFATE. STFATE simulations are executed in sequence,

with the resulting accumulation of dredged material from previous simulations used as initial bathymetry for subsequent simulations. The cycle of short-term processes (by STFATE) continues for the duration of DMP, with intermediate and final conditions of the mound saved for evaluation by the user. More detailed descriptions of the sediment process and how the model simulates them are provided below.

### 4.2.3 Environmental conditions

Environmental conditions that influence morphology of the DMP sites include currents, waves, and water-column density structure. Improvements in the modeling of DMP have been primarily made through improved resolution of hydrodynamics and water column density structure and improved methods for importing results from numerical hydrodynamic and wave transformation models into the MPFATE and STFATE simulations.

Improvements in representing hydrodynamics at DMP sites have been primarily achieved through upgrades to STFATE. In STFATE version 6.1, time-variance in currents at the placement site was incorporated. This feature allows time-varying velocities for either a point measurement (in which case the velocity field is distributed by forcing mass-conservation) or a full velocity field imported from an external numerical model. These enhancements allow a time-varying velocity description at the site which can vary in complexity from simple tidal harmonics, a time-series of velocity measurements, or velocity fields including wind-, tide-, and baroclinic-forcing. ADCIRC currents generated by wind and tide were used in these simulations.

Vertical density gradients primarily influence the descent rate of high-density plumes and settling rate of individual particles. Both of these influences are associated with short-term DMP processes. STFATE version 6.1 introduced improved resolution of the vertical density gradients in the water column, which in turn are available in MPFATE. The GH simulations were performed with uniform water density of 1.025 g/cm3.

### 4.2.4 Boundary conditions and inputs

MPFATE has several input parameters that include a description of the dredged material, vessel size, speed and bearing, hydrodynamic and environmental forcing, and DMP sequence.

The description of the dredged material defines important physical characteristics of the sediments handled by the dredging operation. Physical parameters required for short-term processes at the DMP sites include water content, clump fraction, sediment grain size distribution, sediment mineral density, sediment settling velocity, deposited void ratio, and critical bed shear stress for deposition. The version of MPFATE that was used by Demirbilek et al. (2010) holds the dredged material description constant for a single MPFATE simulation. Varying dredged material properties can be represented through a sequence of MPFATE simulations, each with a constant dredged material description. The approach taken for this study was to represent the dredged material in a mass-averaged sense, such that the material characteristics for each load of a particular vessel were represented as the composite characteristics of the dredged material to be placed within a disposal site.

Often, the objectives of an MPFATE simulation is to determine the distribution of DMP to achieve objectives such as maximum site capacity, avoidance of navigation hazards, minimization of erosion for non-dispersive sites, or minimization of dredged material deposition outside the DMP site boundaries.

The morphological development at a DMP site is highly dependent upon the placement sequence and placement operations prescribed by the dredged material manager. Placement operations that influence DMP site morphology include: vessel velocity (including speed and direction) during placement, maneuvering of the placement vessel during release, distribution of placement locations, and ambient currents. Many of the parameters influencing placement operations in the field are subject to the control of the dredged material manager through the dredging contract. These operational parameters are represented in the model through user input or estimated by internal algorithms in the model (based on the geometry of the site, characteristics of the specified dredging equipment, and typical placement operations).

### 4.2.5 Modifications made to MPFATE

Application of MPFATE and LTFATE in the previous study of dredged material management at GH (Demirbilek et al. 2010) revealed some limitations of the modeling approach at this particular site. In the previous application, MPFATE-estimated dredged material mounds were much more highly concentrated and peaked higher than those observed

historically at these sites. The model deficiencies from that study were attributed to inadequate representation of placement by moving vessels in MPFATE and the neglect of sediment transport during the placement cycle. The changes made to MPFATE during this study to remove these limitations are briefly described next.

MPFATE calls a subset of STFATE code to model the processes of a single DMP operation. The MPFATE version of STFATE is identical in physical process routines, but has slightly different input/output procedures, and exists as a separate code. An error in the representation of moving vessels was identified and corrected in STFATE several years ago, but the error remained in the version called from MPFATE. The error was corrected in STFATE and tested to confirm proper operation when called from MPFATE.

Sediment transport during the DMP sequence was a feature of the legacy code MDFATE. MDFATE simulates DMP for a user-specified period (typically a few weeks to one month) followed by sediment transport on the grid for that same period of time. This cycle repeats for the full duration of the MDFATE simulation. The sediment transport model used in MDFATE is Ackers and White (1973), which was developed for non-cohesive sediment bedload transport in streams. Ackers and White sand transport model is limited in its ability to represent sand transport in coastal and estuarine applications (Gailani et al. 2003). The localized grid (the immediate area surrounding the dredged material mound), the inability to represent cohesive and mixed sediments, and the limited capability to represent sandy sediments impose significant constraints on the MDFATE sediment transport capabilities.

Significant improvements have been made in coastal/estuarine sediment transport methods for both non-cohesive and cohesive sediments. These methods are included in the current version of LTFATE (James et al. 2010; Thanh et. al. 2008). Because LTFATE includes robust 3-D hydrodynamics and sediment transport, the approach chosen in MPFATE development was to link MPFATE and LTFATE, not to imbed a limited version of LTFATE into MPFATE. As part of this study, the first external linkage between MPFATE and LTFATE was developed. The long-term goal for MPFATE is to develop an internal linkage with LTFATE that will offer improved efficiencies in simulation.

The MPFATE-LTFATE linkage was accomplished by mapping the MPFATE and LTFATE grids. Sediment deposition on the MPFATE grid is then transferred as a sediment source (including sediment composition) to LTFATE. The sediment sources are introduced to LTFATE at a user-prescribed time interval (in this study the time interval was approximately one day). By this method, the waves and currents at a DMP site will act continually to redistribute the sediment placed. Note that this coupling is one-way (MPFATE does not receive updated bathymetry from LTFATE at daily intervals). The bathymetry updates to MPFATE were accomplished by stopping the LTFATE simulation at 2-3 month intervals and interpolating the LTFATE bathymetry onto the MPFATE grid. Additional details on the MPFATE-LTFATE coupling are provided in Chapter 5.

## 4.3 LTFATE

### 4.3.1 Model description

The numerical modeling simulations for the far-field sediment transport modeling component of this study were performed with the LTFATE model. The hydrodynamic model in LTFATE is the Environmental Fluid Dynamics Code (EFDC) surface water modeling system (Hamrick 2007a; 2007b; and 2007c). EFDC is a public domain, three-dimensional finite difference model that contains dynamically linked hydrodynamic and sediment transport modules. EFDC can simulate barotropic and baroclinic flow in a water body due to astronomical tides, wind, density gradients, and river inflow. It solves the three-dimensional (3-D), vertically hydrostatic, free surface, turbulence averaged equations of motion. EFDC is extremely versatile, and can be used for 1-D, 2-D-laterally averaged (2-DV), 2-D-vertically averaged (2-DH), or 3-D simulations of rivers, lakes, reservoirs, estuaries, coastal seas, and wetlands.

For realistic representation of horizontal boundaries, the governing equations in EFDC are formulated such that the horizontal coordinates, $x$ and $y$, are curvilinear. To provide uniform resolution in the vertical direction, the sigma (stretching) transformation is used. The equations of motion and transport solved in EFDC are turbulence-averaged, because prior to averaging, although they represent a closed set of instantaneous velocities and concentrations, they cannot be solved for turbulent flows. A statistical approach is applied, where the instantaneous values are decomposed into mean and fluctuating values to enable the solution. Additional terms that represent turbulence are introduced to the equations for the mean flow.

Turbulent equations of motion are formulated to utilize the Boussinesq approximation for variable density. The Boussinesq approximation accounts for variations in density only in the gravity term. This assumption simplifies the governing equations significantly, but may introduce large errors when density gradients are large.

The resulting governing equations, presented below, include parameterized, Reynolds-averaged stress and flux terms that account for the turbulent diffusion of momentum, heat and salt. The turbulence parameterization in EFDC is based on the Mellor and Yamada (1982) level 2.5 turbulence closure scheme, as modified by Galperin et al. (1988), that relates turbulent correlation terms to the mean state variables. The EFDC model also solves several transport and transformation equations for different dissolved and suspended constituents, including suspended sediments, toxic contaminants, and water quality state variables. An overview of the governing equations is given in the following; detailed descriptions of the model formulation and numerical solution technique used in EFDC are provided by Hamrick (2007b). Additional capabilities of EFDC include: 1) simulation of wetting and drying of flood plains, mud flats, and tidal marshes; 2) integrated, near-field mixing zone model; 3) simulation of hydraulic control structures such as dams and culverts; and 4) simulation of wave boundary layers and wave-induced mean currents.

The 3-D, Reynolds-averaged equations of continuity (Equation 4-1), linear momentum (Equations 4-2 and 4-3), hydrostatic pressure (Equation 4-4), equation of state (Equation 4-5) and transport equations for salinity and temperature (Equations 4-6 and 4-7) written for curvilinear-orthogonal horizontal coordinates and a sigma (stretching) vertical coordinate are given by Hamrick (2007b) and repeated below:

$$\frac{\partial(m\varepsilon)}{\partial t}+\frac{\partial(m_y Hu)}{\partial x}+\frac{\partial(m_x Hv)}{\partial y}+\frac{\partial(mw)}{\partial z}=0 \tag{4-1}$$

$$\frac{\partial(mHu)}{\partial t}+\frac{\partial(m_y Huu)}{\partial x}+\frac{\partial(m_x Hvu)}{\partial y}+\frac{\partial(mwu)}{\partial z}-$$
$$(mf+v\frac{\partial(m_y)}{\partial x}-u\frac{\partial m_x}{\partial y})Hv=m_y H\frac{\partial(g\varepsilon+p)}{\partial x}- \tag{4-2}$$
$$m_y(\frac{\partial H}{\partial x}-z\frac{\partial H}{\partial x})\frac{\partial p}{\partial z}+\frac{\partial(mH^{-1}A_v\frac{\partial u}{\partial z})}{\partial z}+Q_u$$

$$\frac{\partial(mHv)}{\partial t}+\frac{\partial(m_y Huv)}{\partial x}+\frac{\partial(m_x Hvv)}{\partial y}+\frac{\partial(mwv)}{\partial z}+$$
$$(mf+v\frac{\partial(m_y)}{\partial x}+u\frac{\partial m_x}{\partial y})Hu=m_x H\frac{\partial(g\varepsilon+p)}{\partial y}- \quad (4\text{-}3)$$
$$m_x(\frac{\partial H}{\partial y}-z\frac{\partial H}{\partial y})\frac{\partial p}{\partial z}+\frac{\partial(mH^{-1}A_v\frac{\partial v}{\partial z})}{\partial z}+Q_v$$

$$\frac{\partial p}{\partial z}=\frac{gH(\rho-\rho_o)}{\rho_o}=gHb \quad (4\text{-}4)$$

$$\rho=\rho(\rho,S,T) \quad (4\text{-}5)$$

$$\frac{\partial(mHS)}{\partial t}+\frac{\partial(m_y HuS)}{\partial x}+\frac{\partial(m_x HvS)}{\partial y}+\frac{\partial(mwS)}{\partial z}=\frac{\partial(\frac{mA_b}{H}\frac{\partial S}{\partial z})}{\partial z}+Q_s \quad (4\text{-}6)$$

$$\frac{\partial(mHT)}{\partial t}+\frac{\partial(m_y HuT)}{\partial x}+\frac{\partial(m_x HvT)}{\partial y}+\frac{\partial(mwT)}{\partial z}=\frac{\partial(\frac{mA_b}{H}\frac{\partial T}{\partial z})}{\partial z}+Q_T \quad (4\text{-}7)$$

where $u$ and $v$ are the mean horizontal velocity components in $(x,y)$ coordinates; $m_x$ and $m_y$ are the square roots of the diagonal components of the metric tensor, and $m = m_x m_y$ is the Jacobian or square root of the metric tensor determinant; $p$ is the pressure in excess of the reference pressure, $\frac{\rho_o gH(1-z)}{\rho_o}$, where $\rho_o$ is the reference density; $f$ is the Coriolis parameter for latitudinal variation; $A_v$ is the vertical turbulent viscosity; and $A_b$ is the vertical turbulent diffusivity. The buoyancy $b$ in Equation 4-4 is the normalized deviation of density from the reference value. Equation 4-5 is the equation of state that calculates water density, $\rho$, as functions of $p$, salinity, $S$, and temperature, $T$.

The sigma (stretching) transformation and mapping of the vertical coordinate is given as:

$$z = \frac{(z^* + h)}{(\xi + h)} \tag{4-8}$$

where $z^*$ is the physical vertical coordinate, and $h$ and $\xi$ are the depth below and the displacement about the undisturbed physical vertical coordinate origin, $z^* = 0$, respectively, and $H = h + \xi$ is the total depth. The vertical velocity in $z$ coordinates, $w$, is related to the physical vertical velocity $w^*$ by:

$$w = w^* - z\left(\frac{\partial \xi}{\partial t} + \frac{u}{m_x}\frac{\partial \xi}{\partial x} + \frac{v}{m_y}\frac{\partial \xi}{\partial y}\right) + (1 - z)\left(\frac{u}{m_x}\frac{\partial h}{\partial x} + \frac{v}{m_y}\frac{\partial h}{\partial y}\right) \tag{4-9}$$

The solutions of Equations 4-2, 4-3, 4-6 and 4-7 require the values for the vertical turbulent viscosity and diffusivity and the source and sink terms. The vertical eddy viscosity and diffusivity, $A_v$ and $A_b$, are parameterized according to the level 2.5 (second-order) turbulence closure model of Mellor and Yamada (1982), as modified by Galperin et al. (1988), in which the vertical eddy viscosities are calculated based on the turbulent kinetic energy and the turbulent macroscale equations. The Mellor and Yamada level 2.5 (MY2.5) turbulence closure model is derived by starting from the Reynolds stress and turbulent heat flux equations under the assumption of a nearly isotropic environment, where the Reynolds stress is generated due to the exchange of momentum in the turbulent mixing process. To make the turbulence equations closed, all empirical constants are obtained by assuming that turbulent heat production is primarily balanced by turbulent dissipation.

The vertical turbulent viscosity and diffusivity are related to the turbulent intensity, $q^2$, turbulent length scale, $l$ and a Richardson number $R_q$ as follows:

$$A_v = \Phi_v q l = 0.4(1 + 36R_q)^{-1}(1 + 6R_q)^{-1}(1 + 8R_q) q l \tag{4-10}$$

$$A_b = \Phi_b q l = 0.5(1 + 36R_q)^{-1} q l \tag{4-11}$$

where $A_v$ and $A_b$ are stability functions that account for reduced and enhanced vertical mixing or transport in stable and unstable vertical,

density-stratified environments, respectively, and the local Richardson number is given as:

$$R_q = \frac{gH\dfrac{\partial b}{\partial z}}{q^2}\frac{l^2}{H^2} \tag{4-12}$$

A critical Richardson number, $R_q$ = 0.20, was found at which turbulence and mixing cease to exist (Mellor and Yamada 1982). Galperin et al. (1988) introduced a length scale limitation in the MY scheme by imposing an upper limit for the mixing length to account for the limitation of the vertical turbulent excursions in stably stratified flows. They also modified and introduced stability functions that account for reduced or enhanced vertical mixing for different stratification regimes.

The turbulence intensity ($q^2$) and the turbulence length scale ($l$) are computed using the following two transport equations:

$$\frac{\partial(mHq^2)}{\partial t}+\frac{\partial(m_y Huq^2)}{\partial x}+\frac{\partial(m_x Hvq^2)}{\partial y}+\frac{\partial(mwq^2)}{\partial z}=\frac{\partial(\dfrac{mA_q\dfrac{\partial q^2}{\partial z}}{H})}{\partial z}+Q_q \tag{4-13}$$
$$+2\frac{mA_v}{H}((\frac{\partial^2 u}{\partial z^2})+(\frac{\partial^2 v}{\partial z^2}))+2mgA_b\frac{\partial b}{\partial z}-2mH(\frac{q^3}{(B_1 l)})$$

$$\frac{\partial(mHq^2 l)}{\partial t}+\frac{\partial(m_y Huq^2 l)}{\partial x}+\frac{\partial(m_x Hvq^2 l)}{\partial y}+\frac{\partial(mwq^2 l)}{\partial z}=$$
$$\frac{\partial(\dfrac{mA_q\dfrac{\partial q^2 l}{\partial z}}{H})}{\partial z}+Q_l+2\frac{mE_1 lA_v}{H}((\frac{\partial^2 u}{\partial z^2})+(\frac{\partial^2 v}{\partial z^2}))+mgE_1E_3lA_b\frac{\partial b}{\partial z} \tag{4-14}$$
$$-H(\frac{q^3}{(B_1)})(1+E_2(\kappa L)^{-2}l^2)$$

The above two equations include a wall proximity function, $W=1+E_2 l(\kappa L)^{-2}$, that assures a positive value of diffusion coefficient $L^{-1}=(H)^{-1}(z^{-1}+(1-z)^{-1}))$. $\kappa$, $B_1$, $E_1$, $E_2$, and $E_3$ are empirical constants with values 0.4, 16.6, 1.8, 1.33, and 0.25, respectively. All terms with $Q$'s ($Q_u$, $Q_v$, $Q_q$, $Q_l$, $Q_s$, $Q_T$) are sub-grid scale sink-source terms that are modeled as sub-grid scale horizontal diffusion. The vertical diffusivity, $A_q$,

is in general taken to be equal to the vertical turbulent viscosity, $A_v$ (Hamrick 2007b).

The vertical boundary conditions for the solutions of the momentum equations are based on the specification of the kinematic shear stresses. At the bottom, the bed shear stresses are computed using the near bed velocity components $(u_1, v_1)$ as:

$$(\tau_{bx}, \tau_{by}) = c_b \sqrt{u_1^2 + v_1^2}(u_1, v_1) \tag{4-15}$$

where the bottom drag coefficient $c_b = (\frac{\kappa}{\ln(\Delta_1 / 2z_o)})^2$, where $\kappa$ is the von Karman constant, $\Delta_1$ is the dimensionless thickness of the bottom layer, $z_o = z_o^*/H$ is the dimensionless roughness height, and $z_o^*$ is roughness height in meters. At the surface layer, the shear stresses are computed using the $u$, $v$ components of the wind velocity $(u_w, v_w)$ above the water surface (usually measured at 10 m above the surface) and are given as:

$$(\tau_{sx}, \tau_{sy}) = c_s \sqrt{u_w^2 + v_w^2}(u_w, v_w) \tag{4-16}$$

where $c_s = 0.001 \frac{\rho_a}{\rho_w}(0.8 + 0.065\sqrt{u_w{}^2 + v_w^2})$ and $\rho_a$ and $\rho_w$ are the air and water densities, respectively. Zero flux vertical boundary conditions are used for the transport equations.

Numerically, EFDC is second-order accurate both in space and time. A staggered grid or C-grid provides the framework for the second-order accurate spatial finite differencing used to solve the equations of motion. Integration over time involves an internal-external mode splitting procedure separating the internal shear, or baroclinic mode, from the external free surface gravity wave, or barotropic mode. In the external mode, the model uses a semi-implicit scheme that allows the use of relatively large time steps. The internal equations are solved at the same time step as the external equations, and are implicit with respect to vertical diffusion. Details of the finite difference numerical schemes used in the EFDC model are given in Hamrick (2007b), and will not be presented in this report.

The generic transport equation solved in EFDC for a dissolved (e.g., chemical contaminant) or suspended (e.g., sediment) constituent having a mass per unit volume concentration $C$, is

$$\frac{\partial m_x m_y HC}{\partial t} + \frac{\partial m_y HuC}{\partial_x} + \frac{\partial m_x HvC}{\partial y} + \frac{\partial m_x m_y wC}{\partial z} - \frac{\partial m_x m_y w_{sc} C}{\partial z} = \frac{\partial}{\partial_x}\left(\frac{m_y}{m_x} HK_H \frac{\partial C}{\partial x}\right) + \frac{\partial}{\partial_y}\left(\frac{m_x}{m_y} HK_H \frac{\partial C}{\partial y}\right) + \frac{\partial}{\partial_z}\left(m_x m_y \frac{K_v}{H} \frac{\partial C}{\partial z}\right) + Q_c \quad (4\text{-}17)$$

where $K_V$ and $K_H$ are the vertical and horizontal turbulent diffusion coefficients, respectively; $w_{sc}$ is a positive settling velocity when $C$ represents the mass concentration of suspended sediment; and $Q_c$ represents external sources or sinks and reactive internal sources or sinks. For sediment, $C = S_j$ , where $S_j$ represents the concentration of the *j-th* sediment class. The solution procedure is the same as that for the salinity and heat transport equations, which use a high-order upwind difference solution scheme for the advection terms (Hamrick 2007b). Although the advection scheme is designed to minimize numerical diffusion, a small amount of horizontal diffusion remains inherent in the numerical scheme. As such, the horizontal diffusion terms in Equation 4-17 are omitted by setting $K_H$ equal to zero.

The sediment transport model in LTFATE is the SEDZLJ sediment transport model (Jones and Lick 2001). SEDZLJ is dynamically linked to EFDC in LTFATE. The SEDZLJ model was designed to directly use the results obtained using SEDFlume. SEDFlume is a field- or laboratory-deployable flume for quantifying site-specific cohesive and mixed (i.e., cohesive and noncohesive) sediment erosion rates (McNeil et al. 1996). SEDZLJ is an advanced sediment bed model that represents the dynamic processes of erosion, bedload transport, bed sorting, armoring, consolidation of fine-grain sediment dominated sediment beds, settling of flocculated cohesive sediment, settling of individual noncohesive sediment particles, and deposition. An active layer formulation is used to describe sediment bed interactions during simultaneous erosion and deposition. The active layer facilitates coarsening during the bed armoring process.

Figure 4-1 shows the sediment mass balance achieved by SEDZLJ. In this figure, $U$ = near bed flow velocity, $\delta_{bl}$ = thickness of layer in which bedload occurs, $U_{bl}$ = average bedload transport velocity, $D_{bl}$ = sediment deposition

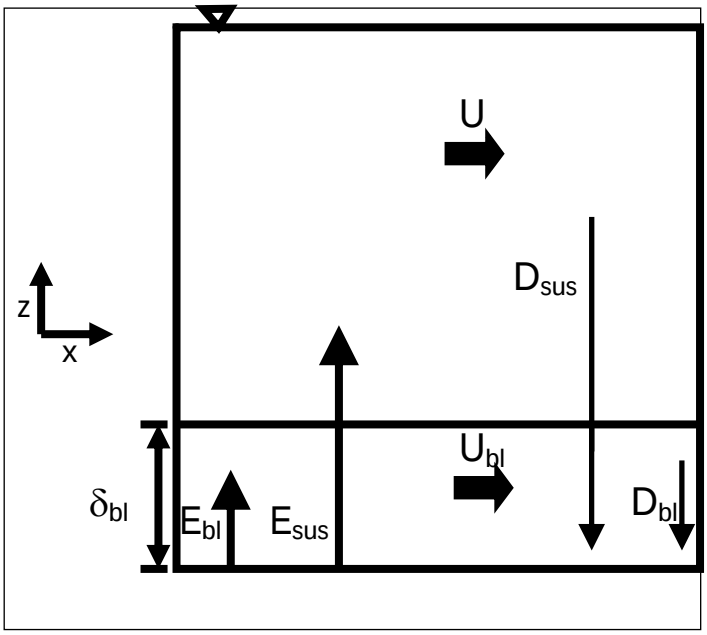


Figure 4-1. Sediment mass balance achieved in SEDZLJ.

rate for the sediment being transported as bedload$E_{bl}$ = sediment erosion rate for the sediment being transported as bedload, $E_{sus}$ = sediment erosion rate for the sediment that is eroded and entrained into suspension, and $D_{sus}$ = sediment deposition rate for suspened sediment. Specific capabilities of SEDZLJ are listed below.

- Whereas a hydrodynamic model is calibrated to account for the total bed shear stress, which is the sum of the form drag due to bed forms and other large-scale physical features and the skin friction (also called the surface friction), the correct component of the bed shear stress to use in predicting sediment resuspension and deposition is the skin friction. The skin friction is calculated in SEDZLJ as a function of the near-bed current velocity and the effective bed roughness. The latter is specified in SEDZLJ as a linear function of the mean particle diameter in the active layer.

  Multiple size classes of both fine-grain (i.e., cohesive) and noncohesive sediments can be represented in the sediment bed. As stated previously, this capability is necessary to simulate coarsening and subsequent armoring of the surficial sediment bed surface during high flow events.

- To correctly represent the processes of erosion and deposition, the sediment bed in SEDZLJ can be divided into multiple layers, some of which are used to represent the existing sediment bed and others that are used to represent new bed layers that form due to deposition during model simulations. Figure 4-2 shows a schematic diagram of this multiple bed layer structure. The graph on the right hand side of this figure shows the variation in the measured gross erosion rate (in units of cm/s) with depth into the sediment bed as a function of the applied skin friction. SEDFLUME was used to measure these erosion rates.

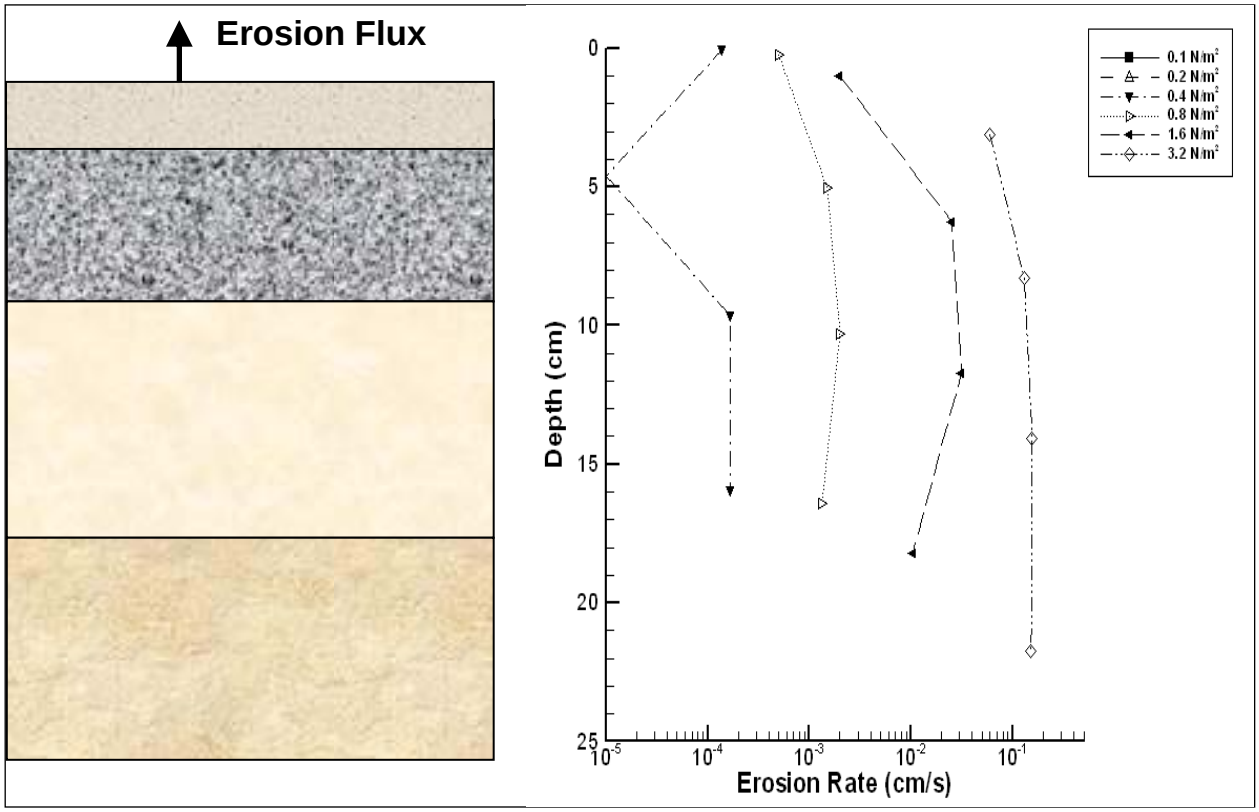


Figure 4-2. Multi-bed layer model used in SEDZLJ.

- Erosion from both cohesive and non-cohesive beds is affected by bed armoring, which is a process that limits the amount of bed erosion that occurs during a high-flow event. Bed armoring occurs in a bed that contains a range of particle sizes (e.g., clay, silt, sand). During a high-flow event when erosion is occurring, finer particles (i.e., clay and silt, and fine sand) tend to be eroded at a faster rate than coarser particles (i.e., medium to coarse sand). The differences in erosion rates of the various sediment particle sizes creates a thin layer at the surface of the sediment bed, referred to as the active layer, that is depleted of finer

particles and enriched with coarser particles. This depletion-enrichment process can lead to bed armoring, where the active layer is primarily composed of coarse particles that have limited mobility. The multiple bed model in SEDZLJ accounts for the exchange of sediment through and the change in composition of this active layer. The thickness of the active layer is normally calculated as a time varying function of the mean sediment particle diameter in the active layer, the critical shear stress for resuspension corresponding to the mean particle diameter, and the bed shear stress. Figure 4-3 shows a schematic of the active layer at the top of the multi-bed layer model used in SEDZLJ.

- SEDZLJ was designed to use the results obtained with SEDFLUME, which is a straight, closed conduit rectangular cross-section flume in which detailed measurements of critical shear stress of erosion and erosion rate as a function of sediment depth are made using sediment cores dominated by cohesive sediment collected at the site to be modeled (McNeil et al. 1996). However, when SEDFLUME results are not available, it is possible to use a combination of values for these parameters available from literature and/or the results of SEDFLUME tests performed at other similar sites. In this case, a detailed sensitivity analysis should be performed to assist in quantifying the uncertainty that results from the use of these non-site specific erosion parameters.
- SEDZLJ can simulate overburden-induced consolidation of cohesive sediments. An algorithm that simulates the process of primary consolidation, which is caused by the expulsion of pore water from the sediment, of a fine-grained, i.e., cohesive, dominated sediment bed is included in SEDZLJ. The consolidation algorithm in SEDZLJ accounts for the following changes in two important bed parameters: 1) increase in bed bulk density with time due to the expulsion of pore water, and 2) increase in the bed shear strength (also referred to as the critical shear stress for resuspension) with time. The latter parameter is the minimum value of the bed shear stress at which measurable resuspension of cohesive sediment occurs. As such, the process of consolidation typically results in reduced erosion for a given excess bed shear stress (defined as the difference between the bed shear stress and the critical shear stress for erosion) due to the increase in the bed shear strength. In addition, the increase in bulk density needs to be represented to accurately account for the mass of sediment (per unit bed area) that resuspends when the bed surface is subjected to a flow-induced excess bed shear stress.

Models that represent primary consolidation range from empirical equations that approximate the increases in bed bulk density and critical shear stress for resuspension due to porewater expulsion (Sanford 2008) to finite difference models that solve the non-linear finite strain consolidation equation that governs primary consolidation in saturated porous media (e.g., Arega and Hayter 2008). An empirical-based consolidation algorithm is included in SEDZLJ.

- SEDZLJ contains a morphologic algorithm that, when enabled by the model user, will adjust the bed elevation to account for erosion and deposition of sediment.

# 5 Sediment Transport Modeling

## 5.1 Introduction

To estimate the short-term and long-term fate of channel deepening sediments, as well as the annual O&M dredging material placed at the SJDS and the PCDS, MPFATE and LTFATE were used to simulate placement, erosion, and transport of dredged material during the dredging window from 15 April 2006 to 14 February 2007. This year was chosen by NWS because it contained a 2-yr return period storm that occurred during the fourth quarter (October – December) of 2006 (Demirbilek et al. 2010). The methodology used to perform this sediment transport modeling is described next. The bathymetry in the navigation channel in the South Reach, Crossover Reach, North Reach, and Hoquiam Reach was deepened to -42 ft (-12.8 m) MLLW in the LTFATE model grid to represent the channel deepening in those reaches.

## 5.2 MPFATE methodology

MPFATE was used to simulate the dredging/placement sequences of Scenarios 1, 2, and 3 which are provided in Table 5-1. Scenarios 1 and 3 represent 4.5 MCY of dredged material and the Scenario 2 represents 3.5 MCY. These volumes were computed assuming that all channels are dredged to -42 ft MLLW; thus they include O&M material plus the sediment required for channel deepening. As of the June 2011 survey (NWS), the cumulative dredging volume is 4.5 MCY (Scenario 1) of which 2.8 MCY is O&M dredging and 1.7 MCY is deepening. The South Reach is assumed to be dredged by hopper dredge Yaquina during the dredging window of mid-April through May. Clamshell dredging is assumed for the reaches inland of the South Reach. Clamshell dredging commences 15 July and continues through 14 February. The Inner Harbor dredging assumes two clamshell dredges and four 3000 CY scows with a total daily production rate of 24,000 CY/day. As indicated in Table 5-1, the dredged material will be placed in the PCDS and SJDS disposal sites (Figure 5-1). The SJDS site is 3000 ft (914 m) long and 800 ft (244 m) wide. For Scenarios 1 and 2, the PCDS priority site (northern portion) is 5000 ft (1524 m) long and 930 ft (284 m) wide, and the south portion is 5000 ft (1524 m) long and 1070 ft (326 m) wide. For Scenario 3, the PCDS was moved to the north 1000 ft (305 m) and the area designated for dredged material placement was the full site (5000 ft (1524 m) long and 2000 ft (610 m) wide).

Table 5-1. Dredged material placement scenarios.

| Month | Dredge Days | Max Monthly Production Volume (CY) | Projected Volume (CY) | SJDS | PCDS | Dredge type |
|---|---|---|---|---|---|---|
| Scenarios 1 and 3 – 4.5 MCY | | | | | | |
| April | 15 | 150,000 | 125,000 | 0 | 125,000 | hopper |
| May | 30 | 300,000 | 249,000 | 0 | 249,000 | hopper |
| June | 29 | | 0 | 0 | 0 | |
| July | 16 | 384,000 | 319,000 | 159,500 | 159,500 | clamshell |
| August | 30 | 720,000 | 598,000 | 299,000 | 299,000 | clamshell |
| September | 29 | 696,000 | 578,000 | 289,000 | 289,000 | clamshell |
| October | 30 | 720,000 | 598,000 | 89,700 | 508,300 | clamshell |
| November | 29 | 696,000 | 578,000 | 86,700 | 491,300 | clamshell |
| December | 30 | 720,000 | 598,000 | 89,700 | 508,300 | clamshell |
| January | 30 | 720,000 | 598,000 | 89,700 | 508,300 | clamshell |
| February | 13 | 312,000 | 259,000 | 38,850 | 220,150 | clamshell |
| Total | 207 | 5,418,000 | 4,500,000 | 1,142,150 | 3,357,850 | |
| Scenario 2 – 3.5 MCY | | | | | | |
| April | 15 | 150,000 | 97,000 | 0 | 97,000 | hopper |
| May | 30 | 300,000 | 194,000 | 0 | 194,000 | hopper |
| June | 29 | | 0 | 0 | 0 | |
| July | 16 | 384,000 | 248,000 | 124,000 | 124,000 | clamshell |
| August | 30 | 720,000 | 465,000 | 232,500 | 232,500 | clamshell |
| September | 29 | 696,000 | 450,000 | 225,000 | 225,000 | clamshell |
| October | 30 | 720,000 | 465,000 | 69,750 | 395,250 | clamshell |
| November | 29 | 696,000 | 450,000 | 67,500 | 382,500 | clamshell |
| December | 30 | 720,000 | 465,000 | 69,750 | 395,250 | clamshell |
| January | 30 | 720,000 | 465,000 | 69,750 | 395,250 | clamshell |
| February | 13 | 312,000 | 202,000 | 30,300 | 171,700 | clamshell |
| Total | 207 | 5,418,000 | 3,500,000 | 888,550 | 2,612,450 | |

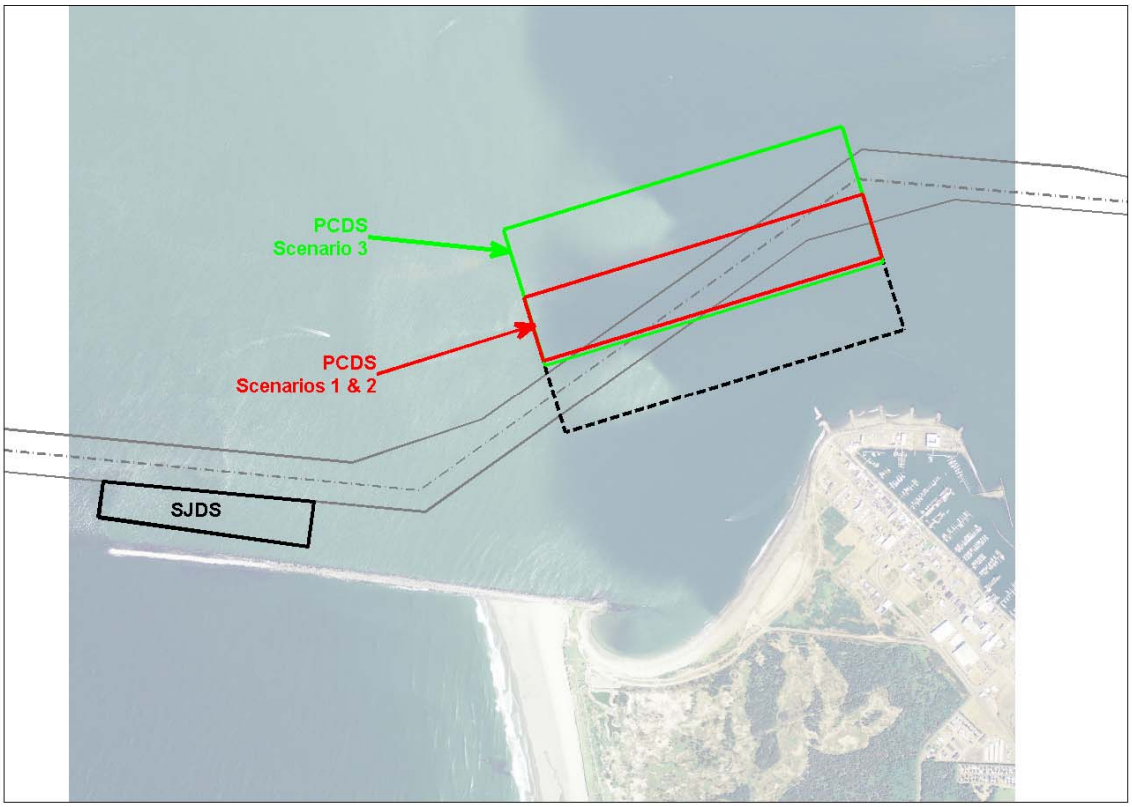


Figure 5-1. South Jetty (SJDS) and Point Chehalis (PCDS) DMP sites.

### 5.2.1 Dredged material characteristics

Sediments in the Grays Harbor federal navigation channel become progressively coarser with distance seaward. The Inner Harbor has approximately 25 percent sand and 75 percent fines, whereas the South Channel has approximately 60 percent sand and 40 percent fines.

The sediment characteristics in the placement vessel (hopper dredge or dump scow) differ from those of the sediment bed due to water entrainment, fracturing of cohesive bed material, and loss of fines during overflow. The dredged material characteristics for placement were estimated to account for these effects.

#### *5.2.1.1 Hopper dredged material*

Sediment composition for the hopper dredge *YAQUINA* was taken from the previous study (Demirbilek et al. 2010) for dredged material coming from the South Channel. The *YAQUINA* practices overflow, which causes the sediment composition in the hopper to be considerably coarser than that of the channel, 92.5 percent sand and 7.5 percent fines. Also due to overflow,

the volume fractions of solids in the hopper were relatively high (62 percent sand and 5 percent fines) resulting in a bulk density (unit mass of sediment and water) in the hopper of 2.12 g/cm$^3$. Each hopper placement released 700 CY of dredged material. Settling velocities of sand was set to 0.034 ft/sec (10.5 mm/sec), consistent with settling velocity of 0.125 mm fine sand, and fines were assigned a settling velocity of 0.0049 ft/sec (1.5 mm/sec) which is consistent with unpublished observations of fine sediment aggregates suspended during dredging operations.

#### *5.2.1.2 Clamshell dredged material*

The dredging from the Crossover Channel to the Inner Harbor is conducted with a clamshell dredge. The average sediment composition for the clamshell-dredged material was determined by weighted averaging of sediment size distributions (from samples) with the estimated dredging quantities by channel reach. The weighted distribution estimates were: Inner Crossover (12 percent), Outer Crossover (18 percent), North Channel (19 percent), Hoquiam (18 percent), and Cow Point (24 percent). The resulting sediment composition was 42 percent sand, 58 percent fines. The fine content in the barge was not segregated into clay or silt fractions. Recent research into aggregation of fine-grained sediment in dredge plumes suggests that little of the fine grained sediment is disaggregated during the dredging process. Instead, the clay and silt particles are more generally aggregated into flocs or denser bed aggregates (Smith and Friedrichs 2011). Settling velocities of sand was set to 0.034 ft/sec (10.5 mm/sec), consistent with settling velocity of 0.125 mm fine sand, and fines were assigned a settling velocity of 0.0049 ft/sec (1.5 mm/sec) which is consistent with unpublished observations of fine sediment aggregates suspended during dredging operations.

Mechanical dredging of fine sediments results in partial fragmentation of the sediment bed and entrainment of water. Both of these factors must be included in describing the dredged material released from the dump scow. First, the water entrained by the mechanical dredge includes water introduced during disturbance and fracturing of the bed, but also the overlying water resulting from underfilled buckets. The entrainment of water or bulking of the sediment is often described by a bulking factor (the ratio of dredged sediment volume to bed volume). Bray et al. (1997) summarize bulking factors determined from mechanical dredging of various sediment types. The Bray et al. (1997) bulking factor for sandy silt is 1.2. Assuming an initial bulk density of the bed of 1.7 g/cm$^3$ (a moderately consolidated mixed

sediment bed), the bulk density of the dredged material would be 1.58 g/cm$^3$.

Due to partial fragmentation of the sediment bed, mechanical dredges often release large bed fragments into the barge. These "clumps" range in size from near that of the bucket down to smaller, sand or gravel sized bed fragments. It is difficult to measure, estimate, or describe these clumps, but they strongly influence the behavior of placed dredged material and must be described in the model. In a memorandum to the New York District by Paul Schroeder and Mike Palermo they outlined a heuristic model for the clump fraction of mechanically dredged fine sediment based on plasticity of the sediment to be dredged. They assert that if the water content of the sediment is less than the liquid limit, then the clump fraction is at most 90 percent. If the water content is higher than 1.8 times the liquid limit, then the clump fraction is zero percent. They further presume that for water contents between these limits, the clump fraction varies linearly. In equation form, the Schroeder-Palermo clump fraction estimate is:

$$f_c = \begin{cases} 0.9 & \dfrac{w}{LL} < 1 \\ \dfrac{81}{40} - \dfrac{9}{8}\dfrac{w}{LL} & 1 \le \dfrac{w}{LL} \le 1.8 \\ 0 & \dfrac{w}{LL} > 1.8 \end{cases} \tag{5-1}$$

For the present study, we do not have the water content or liquid limit of the O&M and new work sediments to be dredged. Therefore, we rely on engineering judgment and historical response of the DMP sites to guide the selection of clump fraction. The O&M dredged material is in the channel for a short period of time and has little time and low overburden to consolidate to a highly compacted state. To represent this material, a clump fraction of 0.10 (10 percent) is assumed. (The mound heights simulated with 10 percent clumps agreed favorably with bed change records at South Jetty.) The sediment bed to be dredged for deepening has been in place for a longer period of time and has historically experienced a higher overburden of overlying sediment. Consequently, we would expect this material to have a lower water content, higher degree of strength, and higher clump fraction. To represent the increased clump content of the combined O&M and new work sediment a scenario with 50 percent clumps was simulated.

Mass fraction of clumps was accounted for the volumetric composition of the dredged material in the barge. Table 5-2 provides the volume fractions, settling velocities, critical stresses for deposition, and depositional void ratios for the clamshell dredged sediments.

Table 5-2. Sediment class descriptions for clamshell dredged material.

| Sediment Class | Volume Fraction | Density ($g/cm^3$) | Settling Velocity ft/s (mm/s) | Depositional Void Ratio | Critical Stress, Deposition $lbf/ft^2$ (Pa) |
|---|---|---|---|---|---|
| 10% clumps | | | | | |
| Clumps | 0.083 | 1.7 | 0.32 (100) | 0.6 | 0.5 (23.9) |
| Sand | 0.134 | 2.65 | 0.034 (10.5) | 0.6 | 0.007 (0.34) |
| Fines | 0.184 | 2.65 | 0.0049 (1.5) | 4.5 | 0.005 (0.24) |
| Free Water* | 0.600 | 1.002 | | | |
| 50% clumps | | | | | |
| Clumps | 0.417 | 1.7 | 0.32 (100) | 0.6 | 0.5 (23.9) |
| Sand | 0.074 | 2.65 | 0.034 (10.5) | 0.6 | 0.007 (0.34) |
| Fines | 0.102 | 2.65 | 0.0049 (1.5) | 4.5 | 0.005 (0.24) |
| Free Water* | 0.407 | 1.002 | | | |

* Free water does not include interstitial water contained in clumps.

### 5.2.2 Placement pattern

The placement sites are intended to temporarily store Grays Harbor dredged material without impacting navigation. One approach towards maximizing temporary storage within the site is to avoid mounding in any particular location. To achieve this goal, the simulations were configured with a placement pattern that distributed the dredged material over the site uniformly. Within each site, transects were created and the along- and cross-transect spacing was adjusted until the model results produced a relatively flat deposit of dredged material on the bottom. The final distribution of release locations is shown in Figure 5-2.

At the Point Chehalis site, along-transect spacing was 180 ft, the cross-transect spacing was 150 ft, and the site buffer distance was 100 ft. This placement pattern resulted in 135 placements per lift and the placement pattern was repeatedly cycled until all dredged material was placed. At the smaller South Jetty site, the placement spacing was the same as Pt. Chehalis, but resulted in only 45 placements per lift.

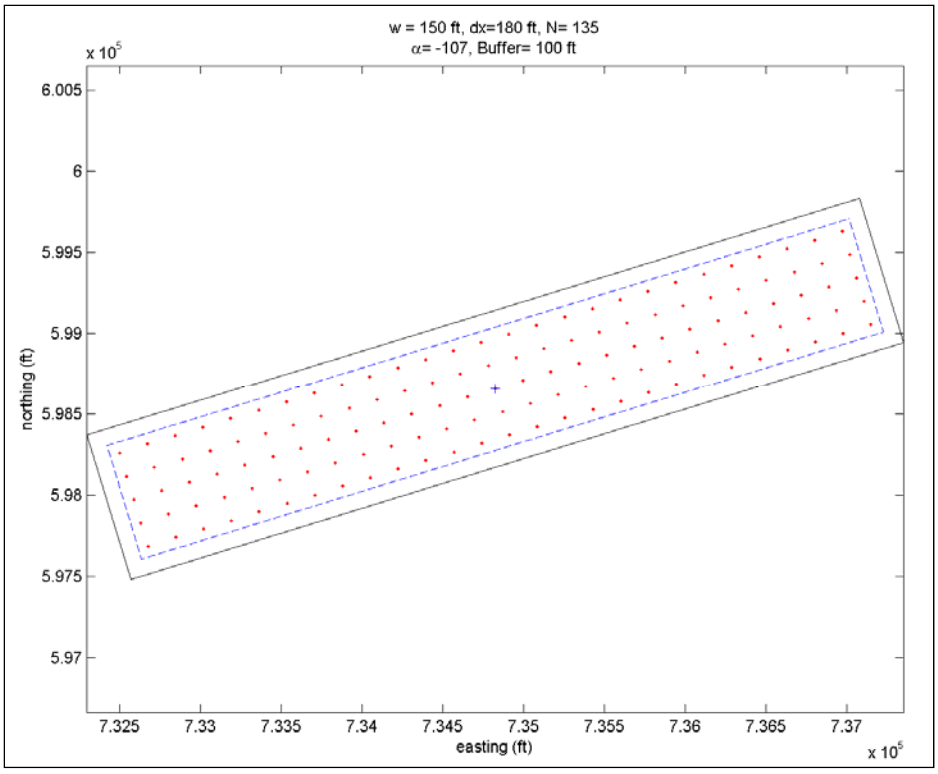


a) Placement pattern for Point Chehalis Site (Scenario 1 & 2).

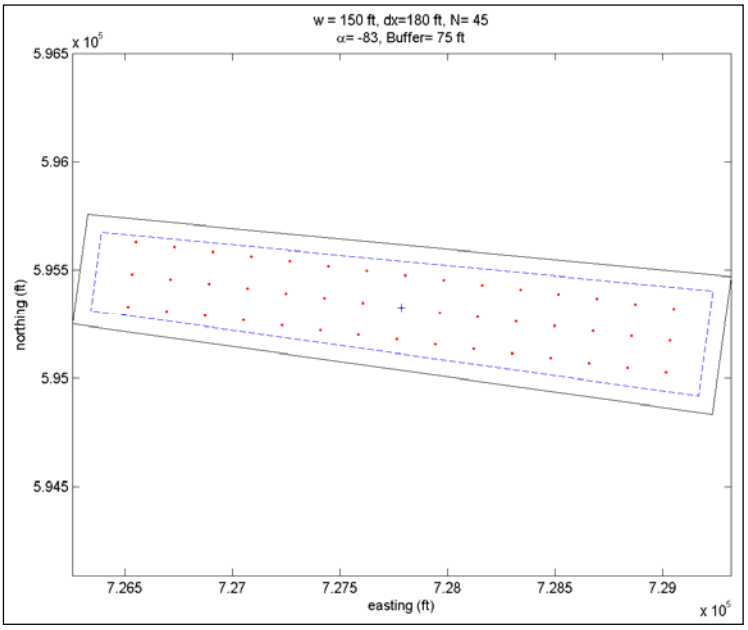


b) Placement pattern for Point Chehalis Site (Scenario 1 & 2).

Figure 5-2. Placement patterns for a) Point Chehalis and b) South Jetty sites. Coordinates are WA state plane, units are ft.

The placement schedule in MPFATE allows for some randomization in placement location, vessel speed, and vessel direction. Placement location was randomly varied within a radius of 50 ft from the target location, vessel speed and direction at time of release was varied between 1-4 knots and ±15 degrees. Hopper and barge placements always had an outbound heading when placing material at both sites.

### 5.2.3 Placement schedule

The DMP schedule was developed from the monthly dredging and production schedules for Scenarios 1, 2 and 3 (Table 5-1). Placements were distributed uniformly over the simulation period. MPFATE simulations were organized as follows: April -May (hopper placement), July - September (barge placement), and October - February (barge placement). The placement start times and intervals are indicated in Table 5-3.

Table 5-3. Placement schedule for MPFATE simulations.

| Simulation Period | Placement Type | Placement Site | Start Date/Time | Placement Interval, hrs |
|---|---|---|---|---|
| Scenarios 1 and 3 | | | | |
| Apr – May | Hopper | PC | 15 April 02:00 | 1.7 |
| Jul-Sep | Barge | PC | 15 July 0:00 | 6.26 |
| Jul-Sep | Barge | SJ | 15 July 0:00 | 6.26 |
| Oct-Feb | Barge | PC | 01 Oct 0:00 | 3.64 |
| Oct-Feb | Barge | SJ | 01 Oct 0:00 | 20.65 |
| Scenario 2 | | | | |
| Apr – May | Hopper | PC | 15 April 02:00 | 2.71 |
| Jul-Sep | Barge | PC | 15 July 0:00 | 8.03 |
| Jul-Sep | Barge | SJ | 15 July 0:00 | 8.03 |
| Oct-Feb | Barge | PC | 01 Oct 0:00 | 4.75 |
| Oct-Feb | Barge | SJ | 01 Oct 0:00 | 27.14 |

### 5.2.4 Hydrodynamic conditions

Hydrodynamic conditions for the MPFATE simulations were extracted from the ADCIRC simulations at the center of each site. These velocities were applied in the STFATE model with a logarithmic vertical distribution and hydraulic roughness of 0.005 ft (0.15 cm). Wave stresses were not

included in the bottom boundary stress calculations for sediment deposition in MPFATE.

### 5.2.5 MPFATE-LTFATE coupling

The MPFATE bathymetry at the beginning of each simulation was interpolated from the LTFATE grid at the corresponding date/time. The results of the MPFATE simulations were externally coupled with LTFATE via a sediment source file. The sediment source file allows LTFATE cells to receive sediment mass at specified times during the simulation. This LTFATE sediment source file was developed from the MPFATE output. Steps in this procedure are outlined below:

1. Mapping of MPFATE cells to LTFATE cells is determined from the MPFATE and LTFATE grids.
2. The MPFATE output file provides the mass, thickness, and sediment class deposited by each placement on the MPFATE grid.
3. The mass in each MPFATE cell is accumulated until the user-specified output interval is reached, then the sediment mass is transferred by the mapping function to the LTFATE grid. This indicates that the sediment mass, sediment density, and sediment class that is to be added to each LTFATE cell, i.e., sediment mass in clumps is decomposed to the constituent sand and fine sediment content of the sediment bed. This procedure is depicted in Figure 5-3 that shows the deposit thickness in the much finer MPFATE grid and the same deposit thickness after it is mapped onto the coarser LTFATE grid.
4. Each source event in the simulation is written to a Matlab binary file format (.MAT) that includes the LTFATE cell indices, date/time, sediment densities, sediment mass, and sediment class.

This procedure is repeated for each MPFATE simulation. Source files for LTFATE may include source input from several MPFATE simulations. In this case, a Matlab routine is executed that combines multiple MPFATE sources and writes an ASCII file containing source instructions for LTFATE. The LTFATE source file only contains sediment that deposited to the bed. Any sediment remaining in suspension at the conclusion of the MPFATE simulation or sediment that exits the MPFATE boundary is excluded.

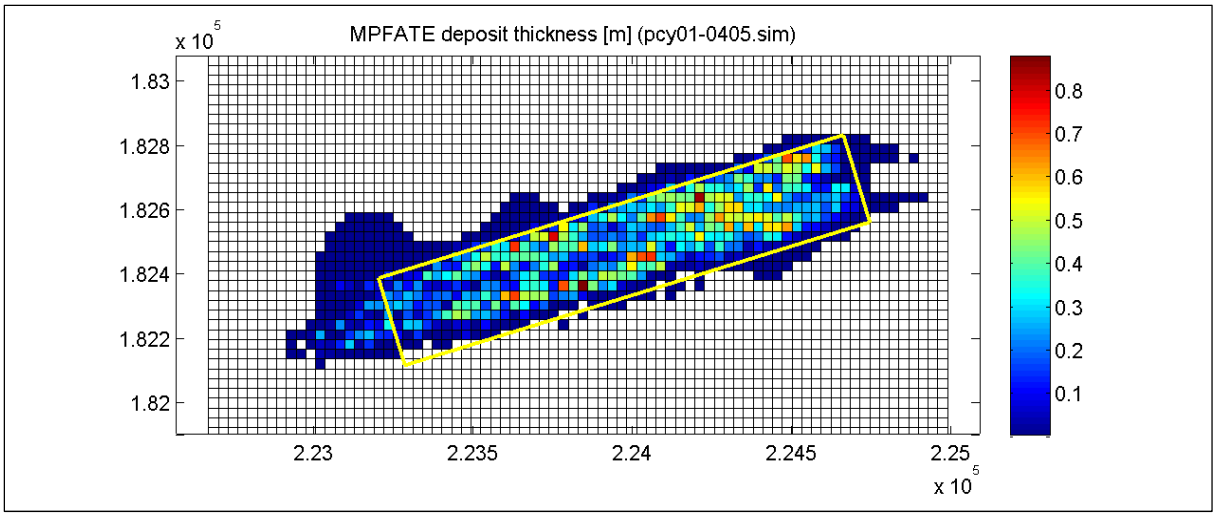


a) MPFATE deposit thickness (Scenario 1, Apr-May Hopper placement).

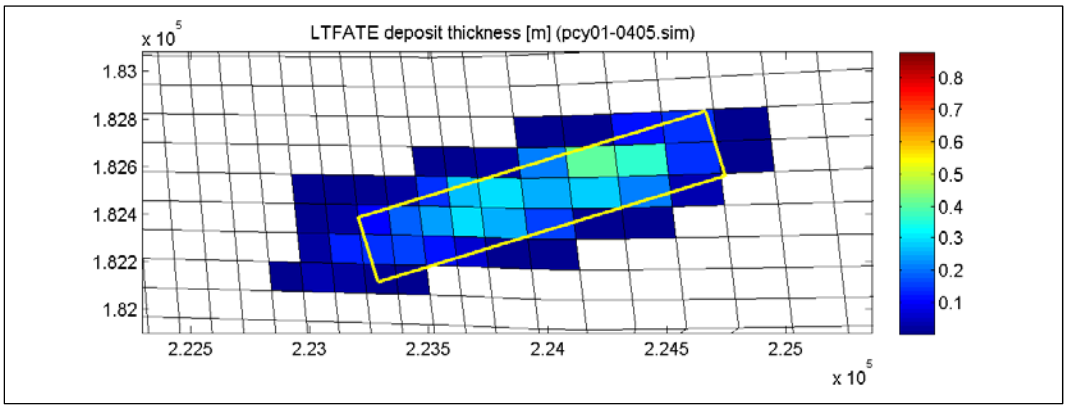


b) LTFATE sediment thickness transferred from MPFATE.

Figure 5-3. Deposit thicknesses (m) for a) MPFATE and b) transferred to LTFATE grid. Grid coordinates are WA state plane, units: meters.

### 5.2.6 MPFATE simulations

A total of 18 MPFATE simulations were executed. Each site (and surrounding area) was represented with a grid of 100x100 ft cells. The 18 simulations represented the various placement rates indicated for Scenarios 1 and 2 and for the 10 percent and 50 percent clump cases. The simulations ran with a 60-second time-step and a 600-second (10-minute) duration. Any sediment that settled to the bed was included in the output file for the grid. Any suspended sediment at the end of the simulation (or that passed a model boundary) is reported to a suspended mass file.

## 5.3 LTFATE methodology

This section describes the application of LTFATE to Grays Harbor, including model setup and a description of the application of LTFATE in this project.

### 5.3.1 Hydrodynamic model setup

A curvilinear-orthogonal grid with 5,406 horizontal grid cells was used to represent the same model domain as that used for CMS-Wave. The model domain and model bathymetry are shown in Figure 5-4. Notice that the model domain extends approximately 15 km up the Chehalis River. The bathymetry data used in constructing this grid were provided by the NWS and National Geophysical Data Center, Coastal Relief Bathymetry Database.

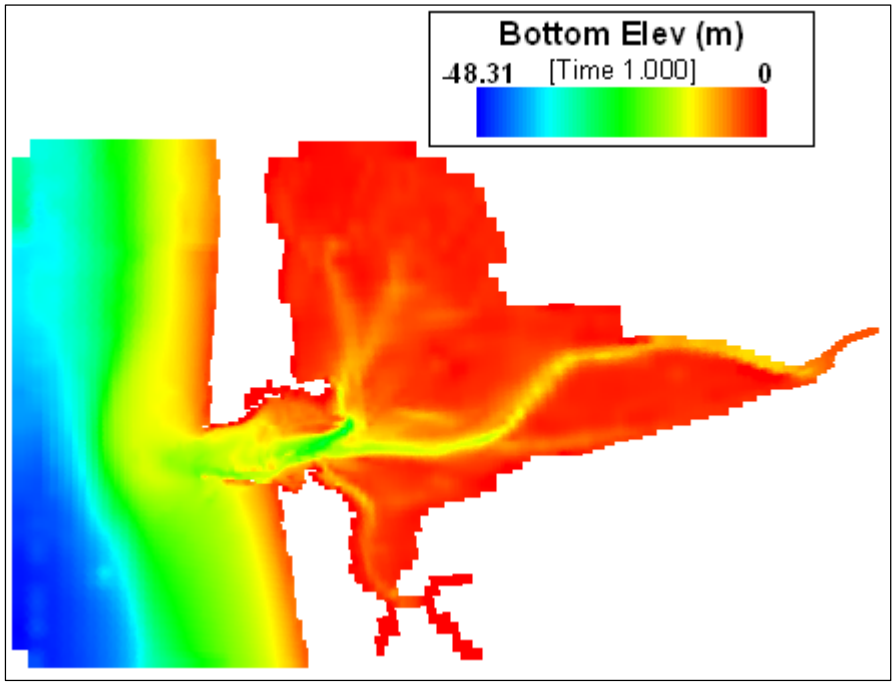


Figure 5-4. LTFATE model domain for Grays Harbor.

As described previously, astronomical tides are the dominant forcing mechanism within Grays Harbor, with riverine flows in the Chehalis River and the Humptulips River secondary in importance. As stated previously, EFDC was driven by ADCIRC simulated tides around the ocean open water boundaries seen in Figure 5-4. Because of the relatively small modeling domain (as quantified by the time it takes for the tidal wave to propagate the full length of the water body being modeled that was relatively short), it

was not necessary to use the radiation-separation boundary condition option in EFDC. Instead, clamped boundary conditions were constructed using the ADCIRC interpolated water surface elevation time series for each grid cell composing the three ocean boundaries.

The river inflows from the Chehalis and Humptulips Rivers are also simulated in the model. The Chehalis River flow record was constructed using the USGS gage 12031000 on the Chehalis River at Porter, WA. This was the closest gage to Grays Harbor that had a continuous period of record from 1 January 1990 to the present. The flow record at Porter was pro-rated to that at the USGS gage 12035100 at Montesano, WA using the ratio of the drainage basin areas at these two gauges. A similar procedure was used to construct the discharge time series for the Humptulips River. The Chehalis River flow record was applied at the upstream most grid cell in the short reach of the Chehalis River included in the model domain. The Humptulips River flow record was applied at a cell at the northeastern corner of North Bay in Grays Harbor. Other physical processes represented by the model include bottom friction and Coriolis acceleration. Wind forcing on the LTFATE domain was neglected, although wind stresses were included in the ADCIRC model run that was used to construct the ocean water surface elevation boundary conditions for LTFATE.

With the meso-tidal conditions in Grays Harbor, the water column is not completely vertically well-mixed for most of the tidal cycle, though measurements by Landerman et al. (2004) showed that the maximum difference between surface and bottom salinities at several nearshore stations was approximately three practical salinity units (psu). No measurements of vertical salinity profiles inside the harbor were found. With such a relatively small salinity gradient, baroclinic flow in Grays Harbor would be minimal. As such, the EFDC model was run in the depth-averaged mode. However, to represent the longitudinal salinity profile that was apparent from the salinity measurements by Hericks and Simpson (2000) the salinity transport module in EFDC was enabled. A salinity of 31 psu was assumed at the three ocean boundaries of the model domain, and salinities of zero psu were used for the river inflows in the Chehalis and the Humptulips Rivers. The calibration and validation of EFDC is described by Demirbilek et al. (2010).

### 5.3.2 Wave stresses and sediment transport

The importance of including wave stresses in the LTFATE simulations was evaluated by calculating bottom shear stresses with and without waves at the center of the SJDS site over the period 15 July – 30 September 2006. The SJDS was selected as it is in a more exposed location and therefore more susceptible to wave forcing. The procedure used for the calculations follows the methods for estimating bottom stress for event selection in Demirbilek et al. (2010). The hydrodynamic conditions were extracted from the ADCIRC simulation of the period at the center of the SJDS. Wave conditions were estimated at the center of the SJDS from the GROW hindcast (offshore conditions) and a lookup table generated from the 2763 CMS-WAVE simulations performed in the study conducted by Demirbilek et al. (2010). The maximum skin friction shear stress was calculated with and without wave forcing by the methods of Soulsby (1997) with an estimated grain roughness of 0.2 mm. Figure 5-5 presents the calculations with and without waves (the solid line indicates no difference). The results suggest that waves contribute significantly to the peak bed stress at the SJ site and should be included in the LTFATE simulation.

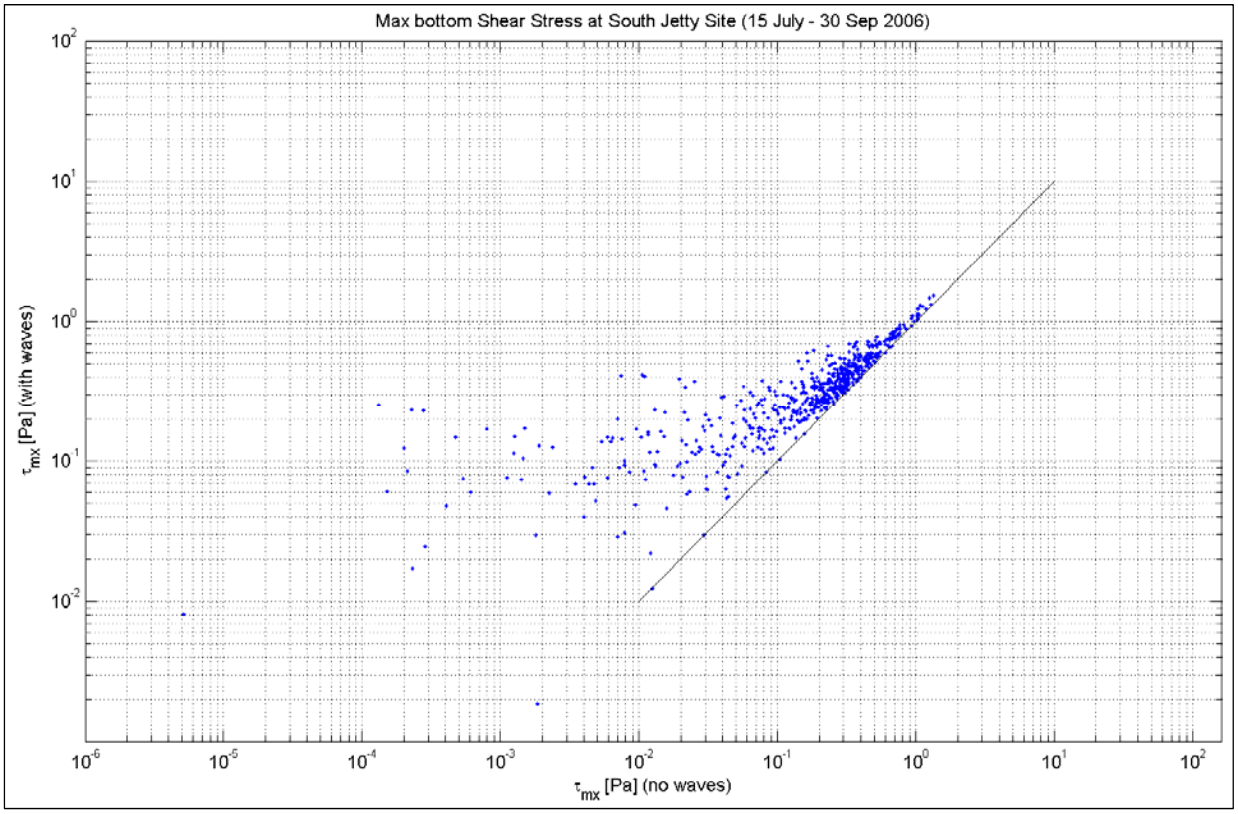


Figure 5-5. Estimated bed stress with and without wave forcing at the center of the SJDS. The solid line indicates no difference.

### 5.3.3 Sediment transport model setup

The SEDZLJ sediment bed model in LTFATE was setup to simulate sediment transport in Grays Harbor using the following information that is described in more detail by Demirbilek et al. (2010):

- Mean settling velocities for flocs of 0.35 mm/sec, and mean settling velocities of bed aggregates of 1.1 mm/sec.
- Size distributions (Percent Volume and Percent Finer) for slurried Grays Harbor dredged material given in Figure 8-6 in Demirbilek et al. (2010).
- Sedflume determined erosion rate versus bed shear stress and the critical shear stress for erosion versus bed density relationship for the representative dredged sediment sample for Cow Point Reach given in Chapter 8 in Demirbilek et al. (2010).
- The regions inside Grays Harbor where marine, river, and mixed marine and river sediments have deposited as reported by Scheidegger and Phipps (1976). Refer to Figure 3-9 in Kraus et al. (2003) for an adaptation of what appears in Scheidegger and Phipps (1976).
- Grain size distributions at multiple locations inside and at the mouth of Grays Harbor, the lower Chehalis River, and offshore locations reported by SAIC (2007) and SAIC (2009). These distributions were used to determine the initial composition of the marine, river, mixed marine and river sediments that were used in cold starts of the SEDZLJ model.

Based on an analysis of all these data it was decided that six sediment grain sizes were needed to adequately represent the wide range of sediment from clay to gravel. The diameters of the six sediment size classes used are 10, 22, 222 (fine sand), 375 (medium sand), 750 (coarse sand), and 4,000 $\mu m$ (fine to very fine gravel). It was assumed that the specific gravity of all six size classes was 2.65. The 10 $\mu m$ size class was used to represent the flocs whose settling speeds were measured in the PICs experiment, whereas the 22 $\mu m$ size class was used to represent the bed aggregates eroded in the Sedflume experiments using the representative GH dredged material. These two cohesive size classes are used to represent the erosion, transport and settling of the fine-grain sediment deposited at the three placement sites. They are not treated as individual sediment particles with the specified diameters. In fact, the specified diameters for these two cohesive size classes are not used in SEDZLJ. The gravel size sediment was needed to represent the range of noncohesive sediment found by SAIC (2009) in the lower Chehalis River.

To be able to determine the fate of the sediment eroded from each placement site, two additional sediment size classes were used to represent the dredge material placed at the two DMP sites – one class for the cohesive fraction and the other for the fine sand fraction. So a total of eight sediment size classes were used in the SEDZLJ modeling. Using these two additional sediment size classes allows determination of the fate of the sediment that is placed at the SJDS and PCDS that erodes from each of the placement sites, specifically how much of the eroded sediment redeposits in the different navigation channel reaches.

Using the available grain size distribution data, five different sediment compositions were used to represent the various sediment types with spatially varying composition in the Grays Harbor model domain. One of the specified sediment compositions is assigned to each grid cell. The five sediment compositions are the following: offshore, marine, mixed marine and river, river, and the Chehalis River. The grain size distributions for the five sediment types (or compositions) are shown in Table 5-4. Each number in this table represents the percentage of each of the six sediment size classes in each sediment type.

Table 5-4. Sediment composition of the five Sedflume cores.

| Sedflume Cores | Sediment Diameter (*μm*) | | | | | |
|---|---|---|---|---|---|---|
| | 10 | 22 | 222 | 375 | 750 | 4000 |
| Riverine Sediments | 13 | 57 | 24 | 5 | 1 | |
| Mixed Riverine and Marine Sediments | 6 | 28 | 62 | 3 | 1 | |
| Marine Sediments | 1 | 1 | 80 | 15 | 2 | 1 |
| Offshore Sediments | 1 | 1 | 95 | 2 | 1 | 0 |
| Chehalis River Sediments | | 53 | 7 | 1 | 22 | 17 |

Seven bed layers were used to represent the sediment bed in each grid cell. The first (top) layer is the active layer through which depositing and eroding sediment passes. The second layer is the layer in which new sediment deposits are placed. This layer is subdivided into a user-specified number of sub-layers that are used to represent consolidating fine-grain dominated sediment. Sediment placed at the PCDS and SJDS over the course of the model simulation are put in the second layer in the grid cells that fall within these two placement sites. The third through seventh bed layer are used to represent the existing sediment bed in each grid cell at

the start of the model simulation. The grain size distribution in each bed layer for a particular sediment type was assumed to be the same, but the critical shear stress and bed density was increased for the lower layers for the cores in which cohesive sediment (i.e., clay and silt size sediment) made up at least 20 percent by mass of the sediment.

Because LTFATE was run in a depth-averaged mode, a Rouse profile was assumed for the vertical suspended sediment concentration profiles for all four noncohesive sediment size classes. This is a customary assumption that is made in modeling the transport of noncohesive sediments and represents the fact that the highest suspended sediment concentration occurs immediately above the bed. This nearbed concentration used in defining the Rouse profile was calculated for each noncohesive sediment size class in each grid cell at each time step as a function of the settling velocity for that sediment size class, and the time-variable depth-averaged suspended sediment concentration, flow depth, and shear velocity. The deposition rate for each noncohesive sediment size class was calculated as the product of the nearbed concentration, the settling velocity, and the probability of deposition for noncohesive sediment.

No measurements of suspended sediment concentrations (SSC) or total suspended solids (TSS) have been made at the USGS gages in the Chehalis and Humptulips Rivers that were used in developing a discharge time series for these two rivers. As such, it was assumed that these rivers transported a constant 100 mg/L concentration of the two cohesive sediment size classes and the finest noncohesive sediment size class.

# 6 Sediment Transport Modeling Results

## 6.1 MPFATE

For this study, the MPFATE simulation results are an intermediate product, used to generate time-varying sediment sources to the grid cells in the LTFATE model that fall within the SJDS and the PCDS. One model result of significance is the quantity of sediment remaining in suspension at the end of each placement simulation. The mass of suspended sediment is not included in the LTFATE source file. The fraction of mass that leaves the placement site in suspension is presented in Table 6-1. Comparing the simulations indicates that clump fraction has a significant influence on the results. With the 10 percent clumping fraction, approximately 65 percent of the sediment leaves the site during placement compared to approximately 35 percent with a clumping fraction of 50 percent. This suggests not only that the model results are sensitive to this difficult to estimate quantity, but also that placement of dredged material from deepening is likely to accumulate within the placement sites at a faster rate than historical trends with O&M material. These two clumping fractions are thought to represent the upper and lower bounds for this parameter. Thus, the sediment source files generated by MPFATE using these two values of the clumping fraction would represent upper and lower bounds for the estimated time varying sediment source being placed in the LTFATE grid cells that fall within the PCDS and SJDS during a LTFATE simulation.

## 6.2 LTFATE

For each of the three dredging scenarios, LTFATE simulated the 10-month dredging window with two MPFATE generated sediment source files, one for 10 percent clumping fraction and the other for 50 percent clumping fraction. The configurations of the placed mounds at the PCDS and the SJDS at the end of the 10-month simulation for Scenarios 1, 2 and 3 are shown in Figures 6-1, 6-2 and 6-3, respectively. The boundaries of the disposal sites are indicated by the two dashed black rectangles, and the solid light grey lines seen in these figures are the boundaries of the navigation channel. As seen in these figures, the heights of the mounds formed using the 10 percent clumping fraction source files are significantly smaller that those formed using the 50 percent clumping fraction source files. The other observable feature seen in comparing these three figures is

that the size of the mounds formed during the Scenario 1 simulations are larger than those that formed during the Scenario 2 simulations, and the mounds formed during the Scenario 3 simulations are the smallest. Both of these findings were expected. The maximum mound heights at the end of the three 10-month LTFATE simulations are shown in Table 6-2.

Table 6-1. Suspended sediment leaving DMP site boundaries during placement (i.e. fraction of mass excluded from LTFATE source).

| Scenario 1, 10% clumps | | | | Scenario 1, 50% clumps | | | |
|---|---|---|---|---|---|---|---|
| Period | Site | Sand | Fines | Period | Site | Sand | Fines |
| Apr-May | PC | 68.4% | 68.2% | Apr-May | PC | 68.4% | 68.2% |
| Jul-Sep | PC | 73.4% | 73.6% | Jul-Sep | PC | 32.5% | 35.1% |
| Jul-Sep | SJ | 43.2% | 53.5% | Jul-Sep | SJ | 17.3% | 18.7% |
| Oct-Feb | PC | 68.0% | 70.8% | Oct-Feb | PC | 31.6% | 33.1% |
| Oct-Feb | SJ | 44.0% | 53.5% | Oct-Feb | SJ | 19.2% | 20.3% |
| Combined | All | 63.7% | 66.6% | Combined | All | 37.7% | 30.3% |
| | | | | | | | |
| Total | All | 65.2% | | Total | All | 33.9% | |
| By Site | PC | 70.2% | | By Site | PC | 38.8% | |
| | SJ | 49.3% | | | SJ | 18.7% | |
| **Scenario 2, 10% clumps** | | | | **Scenario 2, 50% clumps** | | | |
| Period | Site | Sand | Fines | Period | Site | Sand | Fines |
| Apr-May | PC | 69. 6% | 68.1% | Apr-May | PC | 69.6% | 68.1% |
| Jul-Sep | PC | 73.5% | 72.0% | Jul-Sep | PC | 33.5% | 34.4% |
| Jul-Sep | SJ | 47.1% | 52.3% | Jul-Sep | SJ | 18.1% | 19.5% |
| Oct-Feb | PC | 74.2% | 71.5% | Oct-Feb | PC | 36.3% | 35.3% |
| Oct-Feb | SJ | 51.4% | 61.0% | Oct-Feb | SJ | 20.1% | 22.1% |
| Combined | All | 67.6% | 67.1% | Combined | All | 40.2% | 31.7% |
| | | | | | | | |
| Total | All | 67.4% | | Total | All | 35.8% | |
| By Site | PC | 72.1% | | By Site | PC | 41.0% | |
| | SJ | 52.5% | | | SJ | 19.7% | |
| **Scenario 3, 10% clumps** | | | | **Scenario 3, 50% clumps** | | | |
| Period | Site | Sand | Fines | Period | Site | Sand | Fines |
| Apr-May | PC | 69.6% | 72.7% | Apr-May | PC | 69.61% | 72.65% |
| Jul-Sep | PC | 73.6% | 73.0% | Jul-Sep | PC | 34.25% | 34.39% |
| Jul-Sep | SJ | 43.2% | 53.5% | Jul-Sep | SJ | 17.27% | 18.71% |
| Oct-Feb | PC | 71.7% | 71.4% | Oct-Feb | PC | 33.92% | 34.05% |
| Oct-Feb | SJ | 44.0% | 53.5% | Oct-Feb | SJ | 19.17% | 20.28% |
| Combined | All | 65.5% | 66.9% | Combined | All | 39.16% | 30.79% |
| | | | | | | | |
| Total | All | 66.2% | | Total | All | 34.8% | |
| By Site | PC | 71.6% | | By Site | PC | 40.0% | |
| | SJ | 49.3% | | | SJ | 18.7% | |

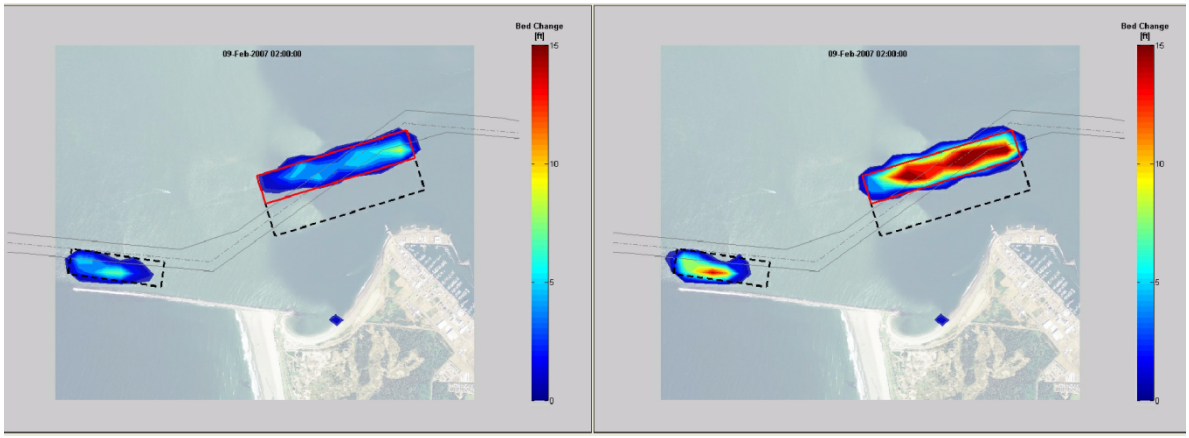


Figure 6-1. Dredge material mounds at end of 10-month LTFATE simulation for Scenario 1 for 10 percent and 50 percent clumping fractions on the left and right frames, respectively. The color legend bar is in units of feet.

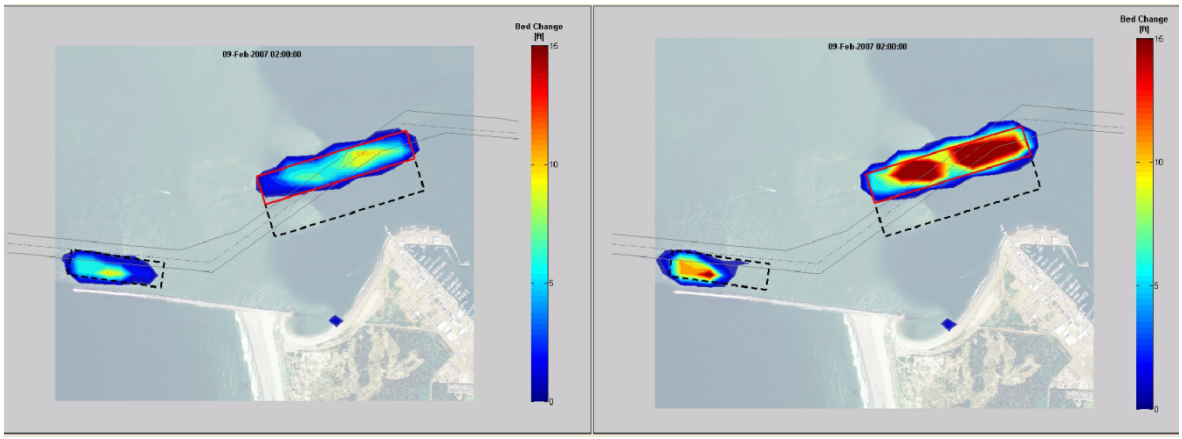


Figure 6-2. Dredge material mounds at end of 10-month LTFATE simulation for Scenario 2 for 10 percent and 50 percent clumping fractions on the left and right frames, respectively. The color legend bar is in units of feet.

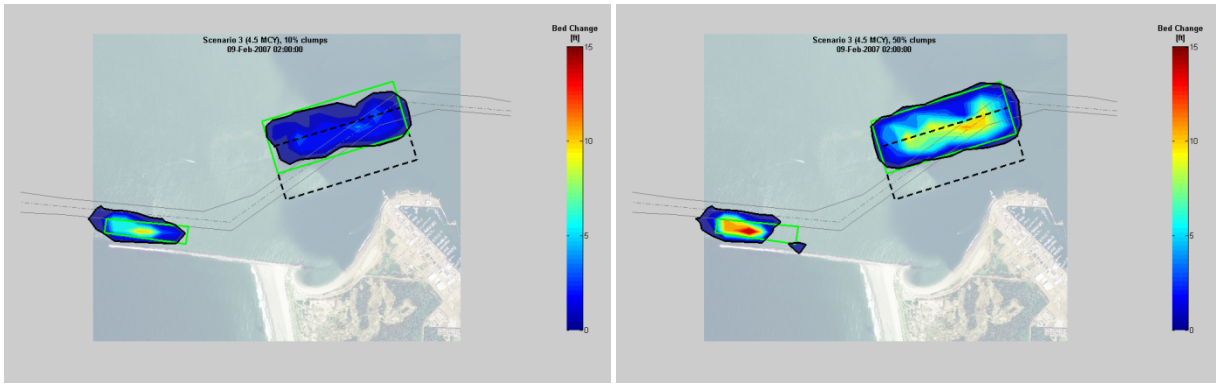


Figure 6-3. Dredge material mounds at end of 10-month LTFATE simulation for Scenario 3 for 10 percent and 50 percent clumping fractions on the left and right frames, respectively. The color legend bar is in units of feet.

Table 6-2. Maximum mound heights (in feet) at end of 10-month LTFATE simulations.

| Clumping Fraction (%) | PCDS | SJDS |
|---|---|---|
| Scenario 1 | | |
| 10 | 8.5 | 9.2 |
| 50 | 20.7 | 15.7 |
| Scenario 2 | | |
| 10 | 7.9 | 6.2 |
| 50 | 16.7 | 13.1 |
| Scenario 3 | | |
| 10 | 4.4 | 11.1 |
| 50 | 11.8 | 18.0 |

Figures 6-4, 6-5 and 6-6 present the depths in the study area at the end of the 10-month simulation. The color scale on the contours indicates depths relative to the maximum dredging depth (-44 ft MLLW at the PCDS and -46 ft MLLW at the SJDS). Green shading indicates depths near -44 ft MLLW; warmer shades indicate depths less than project authorized and cooler shades indicate depths greater than authorized depth. The -44 ft contour is further highlighted with a solid contour line. Figures 6-4, 6-5 and 6-6 indicate that each of the scenarios produces some degree of sedimentation above the maximum project depth. During the 10-month simulation, the maximum widths of navigation channel shallower than the maximum dredging and authorized navigation depths were determined (Table 6-3). Near the SJDS, approximately one-half to two-thirds of the navigation channel was above -46 ft MLLW at some point during the 10-month simulation. Near the PCDS, the smaller placement area of Scenarios 1 and 2 resulted in increased deposit thicknesses (Table 6-2) and increased widths of channel less than the allowable project depth (-44 ft MLLW) compared to the larger placement area of Scenario 3. The results are also relatively sensitive to clump fraction. For Scenarios 1 and 2, the width of channel less than allowable project depth near PCDS increased 2-3 fold with an increase in clump fraction from 10 percent to 50 percent.

Table 6-4 shows the estimated volume of the dredged and placed material that is located in the Entrance, Pt Chehalis, South, and Crossover Channel Reaches at the end of the 10-month LTFATE simulations. As seen in this table, the majority of the placed dredge material is in the two reaches adjacent to the PCDS and the SJDS.

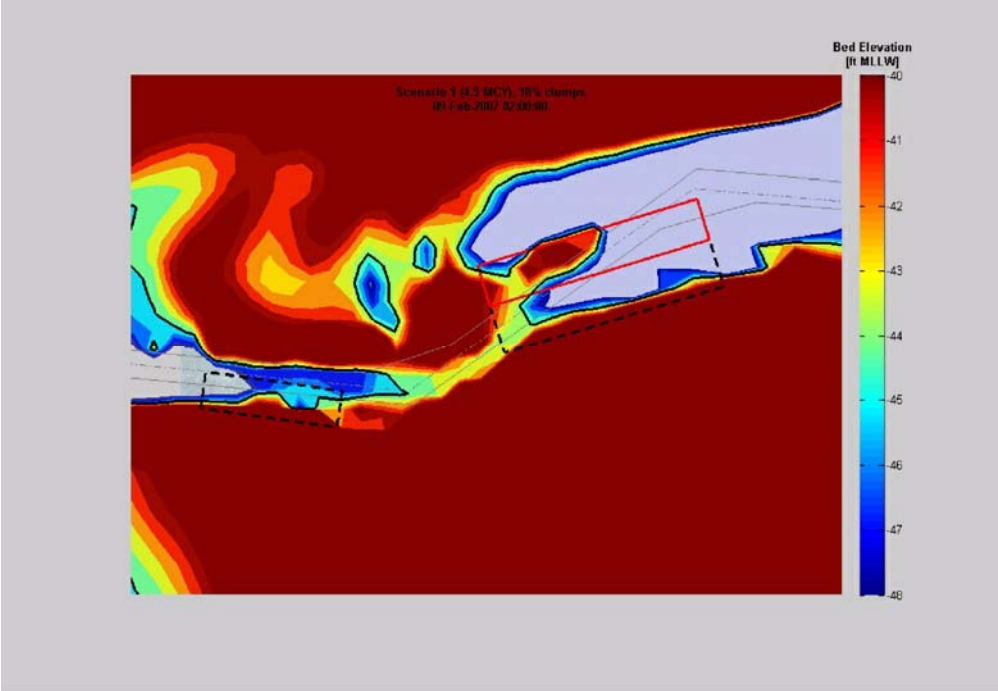


Figure 6-4a. Water depths at end of 10-month LTFATE simulation for Scenario 1 for 10 percent clumping fraction. The color legend bar has units of feet.

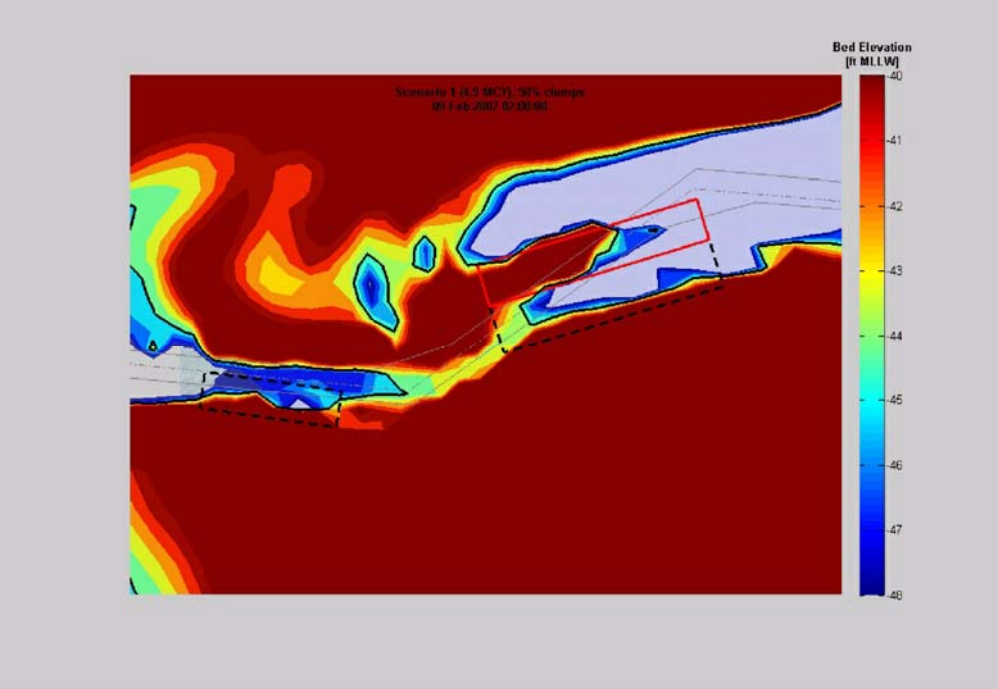


Figure 6-4b. Water depths at end of 10-month LTFATE simulation for Scenario 1 for 50 percent clumping fraction. The color legend bar has units of feet.

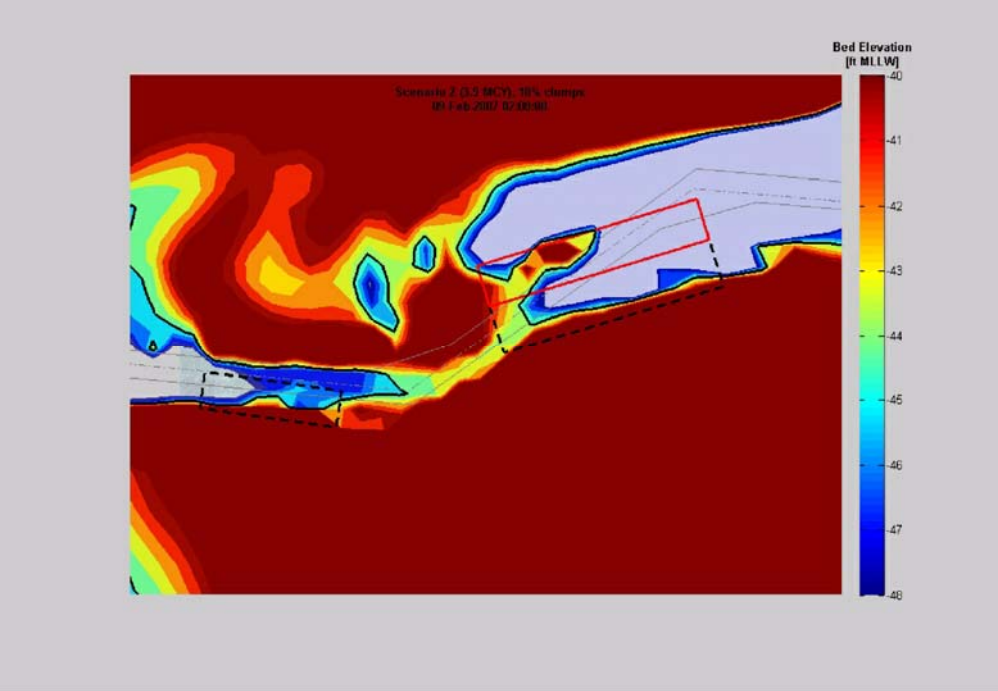


Figure 6-5a. Water depths at end of 10-month LTFATE simulation for Scenario 2 for 10 percent clumping fraction. The color legend bar has units of feet.

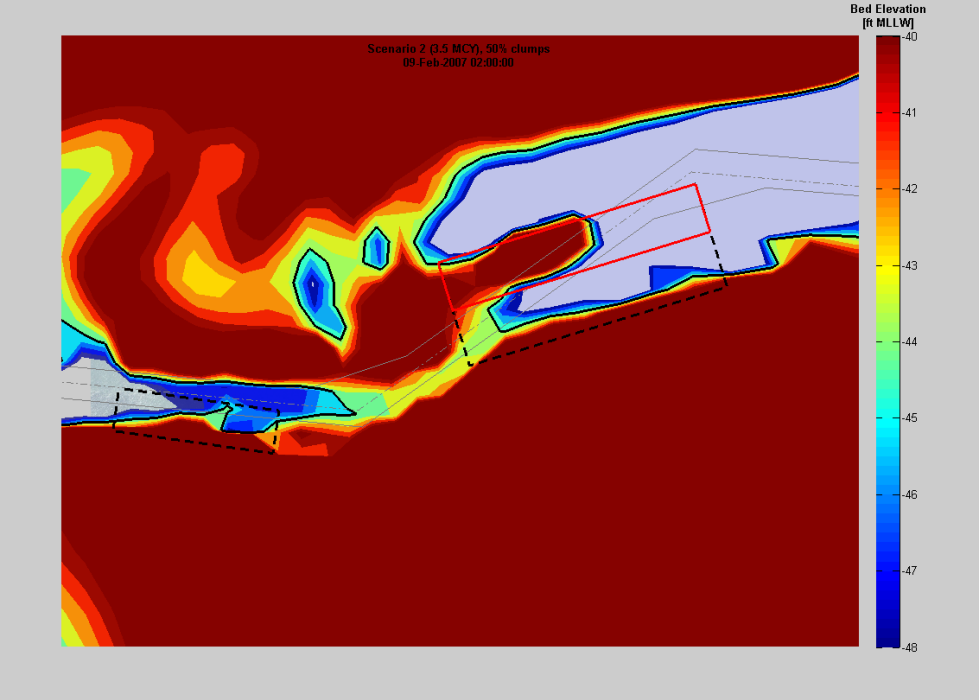


Figure 6-5b. Water depths at end of 10-month LTFATE simulation for Scenario 2 for 50 percent clumping fraction. The color legend bar has units of feet.

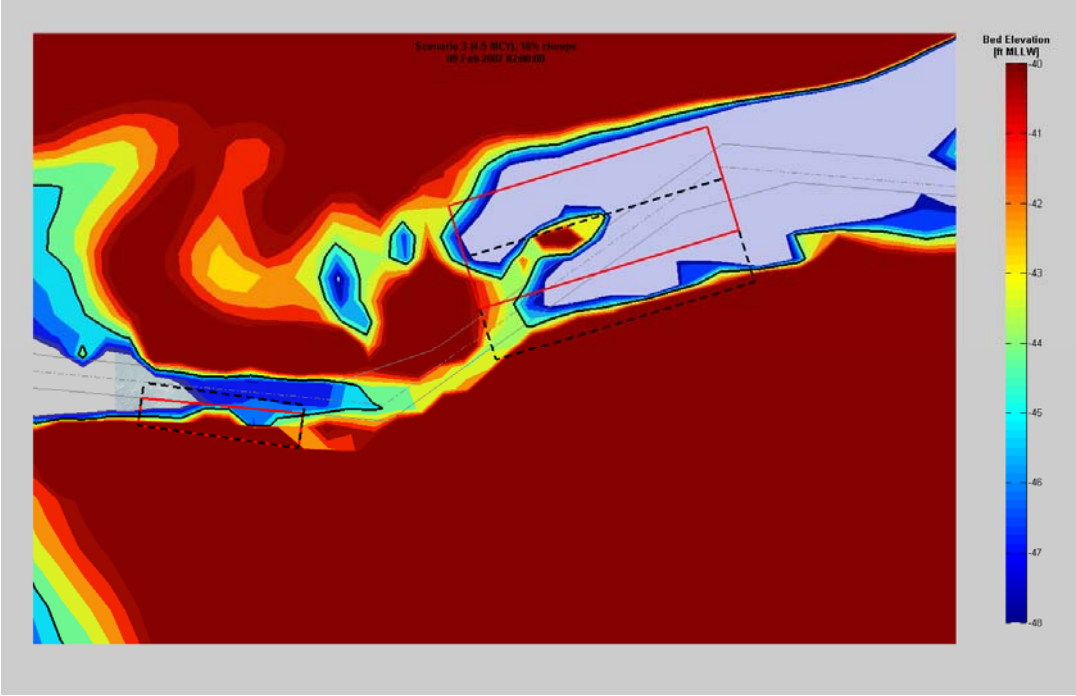


Figure 6-6a. Water depths at end of 10-month LTFATE simulation for Scenario 3 for 10 percent clumping fraction. The color legend bar has units of feet.

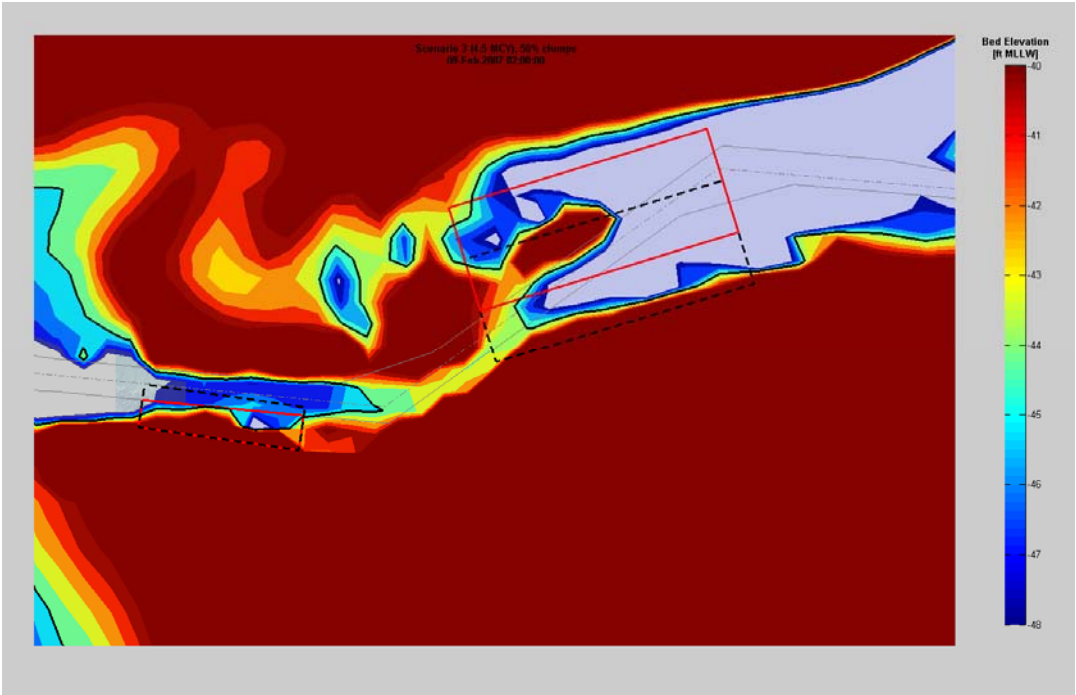


Figure 6-6b. Water depths at end of 10-month LTFATE simulation for Scenario 3 for 50 percent clumping fraction. The color legend bar has units of feet.

Table 6-3. Maximum width of channel with depth less than maximum dredging depth and authorized navigation depth.

| Clumping Fraction (%) | Max Dredging Depth | | Authorized Navigation Depth | |
|---|---|---|---|---|
| | PCDS (-44 ft MLLW) | SJDS (-46 ft MLLW) | PCDS (-40 ft MLLW) | SJDS (-42 ft MLLW) |
| Scenario 1 | | | | |
| 10 | 180 ft (30%) | 350 ft (58%) | 55 ft (5%) | 0 ft (0%) |
| 50 | 450 ft (75%) | 395 ft (66%) | 340 ft (57%) | 0 ft (0%) |
| Scenario 2 | | | | |
| 10 | 130 ft (22%) | 310 ft (52%) | 0 ft (0%) | 0 ft (0%) |
| 50 | 410 ft (68%) | 370 ft (62%) | 270 ft (45%) | 0 ft (0%) |
| Scenario 3 | | | | |
| 10 | 30 ft (5%) | 320 ft (53%) | 0 ft (0%) | 0 ft (0%) |
| 50 | 170 ft (28%) | 395 ft (66%) | 50 ft (8%) | 0 ft (0%) |

Table 6-4. Volume of placed material in channel reaches at the end of the 10-month LTFATE simulations (kCY).

| Clumping Fraction (%) | Entrance Channel | Pt Chehalis Channel | South Channel | Crossover Channel |
|---|---|---|---|---|
| Scenario 1 | | | | |
| 10 | 390 | 400 | 0 | 0 |
| 50 | 500 | 840 | 10 | 0 |
| Scenario 2 | | | | |
| 10 | 300 | 260 | 0 | 0 |
| 50 | 390 | 640 | 10 | 0 |
| Scenario 3 | | | | |
| 10 | 320 | 120 | 10 | 0 |
| 50 | 520 | 350 | 10 | 0 |

# 7 Conclusions and Recommendations

## 7.1 Conclusions

Tidal currents at the SJDS and PCDS are sufficiently strong to transport a significant portion of O&M dredged material away from these sites in suspension (44-53 percent at SJDS and 68-75 percent at PCDS). Sediments dredged during channel deepening are expected to be more highly consolidated, and a higher fraction of clumped sediments is expected in the barge. These clumps have higher settling velocities, and consequently the dredged material from deepening is expected to accumulate more rapidly over time than historically observed for O&M dredged material placement.

Scenarios 1 and 2 with 50 percent clumps caused significant elevation change within the navigation channel. The SJDS and PCDS are situated near naturally deep portions of the navigation channel that ordinarily do not require dredging. Near the PCDS, Scenarios 1 and 2 with 50 percent clumps caused 70-75 percent of the channel width to be shallower than the authorized dredging depth (-44 ft MLLW) at some time during the 10-month simulation. The same simulations resulted in the channel near the SJDS, to have 60-65 percent of the channel to be shallower than the -46 ft MLLW authorized dredging depth. Scenario 3 represented a PCDS that was shifted approximately 1000 ft to the north-northwest and allowed dredged material placement over the entire site. The broader distribution of dredged material placement under Scenario 3 with 50 percent clumps reduced the maximum width of channel shallower than the authorized dredging depth from 75 percent to 28 percent and reduced the width of channel shallower than authorized navigation depth from 57 percent to 8 percent.

## 7.2 Recommendations

Based on the results obtained from the LTFATE modeling, the following recommendations are made:

1. Scenario 3 is the preferred scenario as it produces less accumulation above the authorized dredging depth within the navigation channel over the course of the placement and less channel sedimentation.
2. There is ample capacity in the Scenario 3 PCDS to redistribute the volume of dredged material to reduce direct placement of material in the channel.

Placement operations could be shifted to make more frequent placements in areas of the site with greater capacity or stronger currents.
Under the simulated conditions, the volume of material placed in the SJDS under all scenarios (0.9 – 1.1 MCY) appears to be near the limit of this site without adversely impacting the navigation channel.

The following are recommendations for future studies related to disposal site capacity analyses.

1. Recommend that the MPFATE and LTFATE models be directly (i.e., tightly coupled) coupled to make the use of these models more efficient.
2. Recommend sampling of both the water content and liquid limits of dredged material to permit application of the Schroeder-Palermo method for estimating clump fraction.

# References

Ackers, P. and W.R. White. 1973. Sediment transport: a new approach and analysis. *Journal of Hydraulic Engineering*, 99 (HY11).

Arega, F., and E.J. Hayter. 2008. Coupled Consolidation and Contaminant Transport Model for Simulating Migration of Contaminants through Sediment and a Cap. *Journal of Applied Mathematical Modelling*, 32, 2413–2428.

Bray, R.N., A.D. Bates, and J.M. Land. 1997. *Dredging: A Handbook for Engineers*. Arnold. London.

Bretherton, F. P., and C. J. R. Garrett. 1968. Wave trains in inhomogeneous moving media. *Proceedings Royal Society of London* A(302):529-554.

Collins, J. I. 1972. Prediction of shallow water spectra. *Journal of Geophysical Research* 77(15):2693-2707.

Demirbilek, Z., and V. Panchang. 1998. CGWAVE: A coastal surface-water wave model of the mild-slope equation. *Technical Report CHL-98-26*. Vicksburg, MS: U.S. Army Engineer Waterways Experiment Station.

Demirbilek, Z., L. Lin, J. Smith, E. Hayter, E. Smith, J.Z. Gailani, and G.J. Norwood. 2010. Waves, hydrodynamics, and sediment transport modeling at Grays Harbor, WA. *ERDC/CHL TR-10-13*, U.S. Army Engineer Research and Development Center, Vicksburg, MS.

Demirbilek, Z., and C.L. Vincent. 2010. Wave Mechanics, Part II-1. *Coastal Engineering Manual*, U.S. Army Corps of Engineers.

Demirbilek, Z., and J. Rosati. 2011. Verification and Validation of the Coastal Modeling System, Report 1: Executive Summary. *Technical Report ERDC/CHL TR-11-10*, U.S. Army Engineer Research and Center, Vicksburg, MS.

Flather, R.A. 1988. A numerical model investigation of tides and diurnal-period continental shelf waves along Vancouver Island. *Journal of Physical Oceanography*, 18:115-139.

Gailani, J.Z., S.J. Smith, N.C. Kraus, D.D. McGee, E.B. Hands, C.J. Mayers, H.R. Moritz, H.P. Moritz, M.D. Siipola, D.B. Slocum, M.R. Hyrnes, F. Li, T.L. Dibble, W.H. Hollings, C.R. Lund, C.K. Sollit, and D.R. Standley. 2003. Monitoring dredged material disposal at the mouth of the Columbia River. Washington/Oregon, USA. *ERDC/CHL TR- 03-5*. Vicksburg, MS: U.S. Army Engineer Research and Development Center.

Galperin, B., L.H. Kantha, S. Hassid, and A. Rosati. 1988. A quasi-equilibrium turbulent energy model for geophysical flows. *J. Atmos. Sci.,* **45**, 55-62.

Hamrick, J.M. 2007a The Environmental Fluid Dynamics Code User Manual: US EPA Version 1.01. Tetra Tech, Inc., Fairfax, VA.

Hamrick, J.M. 2007b. The Environmental Fluid Dynamics Code Theory and Computation. Volume 1: Hydrodynamics and Mass Transport. Tetra Tech, Inc., Fairfax, VA.

Hamrick, J.M. 2007c. The Environmental Fluid Dynamics Code Theory and Computation. Volume 2: Sediment and Contaminant Transport and Fate. Tetra Tech, Inc., Fairfax, VA.

Hericks, D.B. and D.P. Simpson. 2000. Grays Harbor Estuary Physical Dynamics Study, Final Data Report: September 11, 1999-November 17, 1999. Pacific International Engineering, Edmonds, WA.

James, S.C., C.A. Jones, M.D. Grace, and J.D. Roberts. 2010. Advances in sediment transport modeling. *Journal of Hydraulic Research*, 48: 6, 754-763.

Johnson, B.H. 1990. User's guide for models of dredged material disposal in open water. *Technical Report D-90-5*, U.S. Army Engineer Waterways Experiment Station, Vicksburg, MS.

Johnson, B.H. and M.T. Fong. 1995. Development and Verification of Numerical Models for Predicting the Initial Fate of Dredged Material Disposed in Open Water, Report 2: Theoretical Developments and Verification Results. *Technical Report DRP-93-1*, U.S. Engineer Waterways Experiment Station, Vicksburg, MS.

Jones, C.A., and W. Lick. 2001. SEDZLJ: A Sediment Transport Model. *Final Report*. University of California, Santa Barbara, California. May 29, 2001.

Kolar, R.L., W.G. Gray, and J.J. Westerink. 1993. An Analysis of the Mass Conserving Properties of the Generalized Wave Continuity Equation. *Proceedings of the IX International Conference on Computational Methods in Water Resources*, T. Russell et al. Eds., Denver, CO.

Kraus, N.C., and H.T. Arden, eds. 2003. North Jetty Performance and Entrance Navigation Channel Maintenance, Grays Harbor, Washington. *ERDC/CHL TR-03-12*, Coastal and Hydraulics Laboratory, U.S. Army Engineer Research and Development Center, Vicksburg, MS.

Landerman, L.A., C.R. Sherwood, G. Gelfenbaum, J. Lacy, P. Ruggiero, D. Wilson, T. Chisholm, and K. Kurrus. 2004. Grays Harbor Sediment Transport Experiment Spring 2001—Data Report. *Data Series 98*, U.S. Geological Survey, Reston, Virginia.

Le Provost, C., M.L. Genco, F. Lyard, P. Vincent, and P. Canceill. 1994. Spectroscopy of the world tides from a hydrodynamic-finite element model, *Journal of Geophysical Research*, 99(Cl2), 777-797.

Lin, L., and R.-Q. Lin. 2004a. Wave Breaking Function. *Proceedings 8th International Workshop on Wave Hindcasting and Prediction*. Oahu, Hawaii: North Shore. November 14-19.

Lin, L., and R.-Q. Lin. 2004b. Wind Input Function. *Proceedings 8th International Workshop on Wave Hindcasting and Prediction*. North Shore, Oahu, Hawaii. November 14-19.

Lin, L., H. Mase, F. Yamada, and Z. Demirbilek. 2006. Wave-action balance equation diffraction (WABED) model: Tests of wave diffraction and reflection at inlets. *Technical Note ERDC/CHL CHETN-III-73*. U.S. Army Engineer Research and Development Center, Vicksburg, MS.

Lin, L., Z. Demirbilek, H. Mase, J. Zheng, and F. Yamada. 2008. CMS-Wave: A Nearshore Spectral Wave Processes Model for Coastal Inlets and Navigation Projects. *Technical Report ERDC/CHL TR-08-13*, Coastal and Hydraulics Laboratory, U.S. Army Engineer Research and Center, Vicksburg, MS.

Lin, L., Z. Demirbilek, R. Thomas, and J. Rosati, III. 2011. Verification and Validation of the Coastal Modeling System, Report 2: CMS-Wave. *Technical Report ERDC/CHL TR-11-10*, Coastal and Hydraulics Laboratory, U.S. Army Engineer Research and Center, Vicksburg, MS.

Luettich, R.L., J.J. Westerink, and N.W. Scheffner. 1992. ADCIRC: An advanced three-dimensional circulation model for shelves, coasts, and estuaries, Report l: Theory and methodology of ADCIRC-2DDl and ADCIRC_3DL. *Technical Report DRP-92-6*, U.S. Anny Engineer Waterways Experiment Station, Vicksburg, MS.

Luettich, R.A., and J.J. Westerink. 2004. Formulation and Numerical Implementation of the 2D/3D ADCIRC Finite Element Model Version 44.XX. Internal Report. available at http://www.adcirc.org/adcirc_theory_2004_12_08.pdf.

Luettich, R.A., and J.J. Westerink. 2004. Hurricane Storm Surge Simulations Using the ADCIRC CoastalOcean Hydrodynamic Model. *58th Interdepartmental Hurricane Conference*, Charleston, SC.

Mase, H. 2001. Multidirectional random wave transformation model based on energy balance equation. *Coastal Engineering,* 43(4):317-337 JSCE.

Mase, H., H. Amamori, and T. Takayama. 2005a. Wave prediction model in wave-current coexisting field. *Proceedings 12th Canadian Coastal Conference* (CD-ROM).

Mase, H., K. Oki, T.S. Hedges, and H.J. Li. 2005b. Extended energy-balance-equation wave model for multidirectional random wave transformation. *Ocean Engineering,* 32(8-9):961-985.

McNeil, J., C. Taylor, and W. Lick. 1996. Measurements of erosion of undisturbed bottom sediments with depth. *Journal of Hydraulic Engineering*, 122(6), 316-324.

Mellor, G.L., and T. Yamada. 1982. Development of a turbulence closure model for geophysical fluid problems. *Rev. Geophys. Space Phys.*, 20, 851-875.

Nwogu, O., and Z. Demirbilek. 2001. BOUSS-2D: A Boussinesq wave model for coastal regions and harbors. *Technical Report ERDC/CHL TR-01-25*, Coastal and Hydraulics Laboratory, U.S. Army Engineer Research and Development Center, Vicksburg, MS.

SAIC, 2007. Grays Harbor Navigational Channel Maintenance Dredging, Grays Harbor, WA. *FY06-07 Dredged Material Characterization Data Report-FINAL*, Bothell, Washington.

SAIC, 2009. Dredged Material Characterization for Grays Harbor Navigational Channel Maintenance Dredging Grays Harbor, WA. *FY08–09 Dredged Material Characterization Data Report Final*, Bothell, Washington.

Sanford, L.P. 2008. Modeling a dynamically varying mixed sediment bed with erosion, deposition, bioturbation, consolidation, and armoring. *Computers & Geosciences*, 34(10): 1263-1283.

Scheidegger, K.F., and J.B. Phipps. 1976. Dispersal Patterns of Sands in Grays Harbor Estuary, Washington. *Journal of Sedimentary Petrology*, 46(1), 163-166.

Smith, S. J., and C.T. Friedrichs. 2011. Size and settling velocities of cohesive flocs and suspended sediment aggregates in a trailing suction hopper dredge plume. *Continental Shelf Research*. 31: S50-S63.

Soulsby, R. L. 1997. *Dynamics of Marine Sands*. Thomas Telford. London.

Thanh, P.X.H., M.D. Grace, and S.C. James. 2008. Sandia National Laboratories Environmental Fluid Dynamics Code: Sediment Transport User Manual. *SAND2008-5621*. Sandia National Laboratories, Livermore, CA.

Westerink, J. J., J.C. Muccino and R.A. Luettich. 1992. Resolution requirements for a tidal model of the Western North Atlantic and Gulf of Mexico, Computational Methods in Water Resources IX, Volume 2: Mathematical Modeling in Water Resources, T. F. Russell et al., [eds], Computational Mechanics Publications, Southampton, UK, pp. 669-674.

Westerink, J.J., R.A. Luettich, Jr. and N.W. Scheffner. 1993. ADCIRC: an advanced three-dimensional circulation model for shelves coasts and estuaries, report 3: development of a tidal constituent data base for the Western North Atlantic and Gulf of Mexico, *Dredging Research Program Technical Report DRP-92-6*, U.S. Army Engineers Waterways Experiment Station, Vicksburg, MS, 154p.

Whitham, G. B. 1974. *Linear and nonlinear waves*. New York, NY: John Wiley.

Wikramanayake, P.N., and O.S. Madsen. 1994a. Calculation of suspended sediment transport by combined wave-current flows. *Contract Report DRP-94-7*, U.S. Army Engineer Waterway Experiment Station, Vicksburg, MS, USA.

Wikramanayake, P.N., and O.S. Madsen. 1994b. Calculation of movable bed friction factors. *Contract Report DRP-94-5*, U.S. Army Engineer Waterway Experiment Station, Vicksburg, MS, USA.

# REPORT DOCUMENTATION PAGE

*Form Approved*
*OMB No. 0704-0188*



| **1. REPORT DATE** *(DD-MM-YYYY)* | **2. REPORT TYPE** | **3. DATES COVERED** *(From - To)* |
|---|---|---|
| September 2012 | Final TR | |

**4. TITLE AND SUBTITLE**

Dredged Material Placement Site Capacity Analysis for Navigation Improvement Project at Grays Harbor, WA

**5a. CONTRACT NUMBER**

**5b. GRANT NUMBER**

**5c. PROGRAM ELEMENT NUMBER**

**6. AUTHOR(S)**

Earl Hayter, Jarrell Smith, David Michalsen, Zeki Demirbilek, and Lihwa Lin

**5d. PROJECT NUMBER**

**5e. TASK NUMBER**

**5f. WORK UNIT NUMBER**

**7. PERFORMING ORGANIZATION NAME(S) AND ADDRESS(ES)**

U.S. Army Engineer Research and Development Center, Coastal and Hydraulics Laboratory, 3909 Halls Ferry Road, Vicksburg, MS 39180-6199

**8. PERFORMING ORGANIZATION REPORT NUMBER**

ERDC/CHL TR-12-18

**9. SPONSORING / MONITORING AGENCY NAME(S) AND ADDRESS(ES)**

U.S. Army Corps of Engineers Seattle District
P.O. Box 3755
Seattle, WA 98124-3755

**10. SPONSOR/MONITOR'S ACRONYM(S)**

**11. SPONSOR/MONITOR'S REPORT NUMBER(S)**

**12. DISTRIBUTION / AVAILABILITY STATEMENT**

**13. SUPPLEMENTARY NOTES**

**14. ABSTRACT**

The U.S. Army Engineer District, Seattle requested that the U.S. Army Engineer Research and Development Center, Coastal and Hydraulics Laboratory perform a numerical modeling study for the purpose of performing a dredged material placement (DMP) site capacity analysis for a Navigation Improvement Project for the Federal Navigation Project at Grays Harbor (GH), WA. The project would deepen the inner harbor channel reaches up to two additional feet to reach the authorized project depth of -38 feet. This would require dredging up to an additional 1.7 million cubic yards (MCY) in addition to the 2.8 MCY available for dredging through the Corps O&M program. A project goal is to maximize the dredge volume capacity within existing open water sites while ensuring navigation safety. This study provides estimate of the short-term and long term fate of channel deepening sediments as well as the annual O&M dredge material placed at the DMP sites in the entrance channel to GH. The model simulations indicated a) potential navigation obstruction for the scenario with additional 2.0 MCY; b) potential obstruction for the scenario with additional 1.0 MCY; and c) channel obstructions were significantly reduced at the PCDS for Scenario 3 where the maximum channel obstruction was 170 ft. Two recommendations are made: a) Scenario 3 is preferred as it produces a minimal obstruction to the navigation channel and less channel sedimentation; and b) Modify placement strategy at the SJDS by placing more material in the eastern half than in the western half of the site rather than the uniform placement strategy used at present.

**15. SUBJECT TERMS**

Channel deepening
Dredged material placement site
Dredged material placement
Dredge volume capacity
Federal navigation project at Grays Harbor, WA
Hydrodynamics and waves
Sediment transport modeling

| **16. SECURITY CLASSIFICATION OF:** | | | **17. LIMITATION OF ABSTRACT** | **18. NUMBER OF PAGES** | **19a. NAME OF RESPONSIBLE PERSON: Zeki Demirbilek** |
|---|---|---|---|---|---|
| **a. REPORT** | **b. ABSTRACT** | **c. THIS PAGE** | | | **19b. TELEPHONE NUMBER** *(include area code)* |
| Unclassified | Unclassified | Unclassified | Unclassified | 78 | (601) 634-2834 |